Essential role of *Cables2* for gastrulation of the mouse embryo

マウス原腸胚形成における *Cables2* の役割

2017

筑波大学グローバル教育院

School of the Integrative and Global Majors in University of Tsukuba

Ph.D Program in Human Biology

DINH THI HUONG TRA

筑 波 大 学
University of Tsukuba

博 士 （人間生物学） 学 位 論 文
PhD dissertation in Human Biology

Essential role of *Cables2* for gastrulation of the mouse embryo

マウス原腸胚形成における *Cables2* の役割

2017

筑波大学グローバル教育院

School of the Integrative and Global Majors in University of Tsukuba

Ph.D Program in Human Biology

DINH THI HUONG TRA

Abbreviations

A-P	anterior - posterior
AVE	anterior visceral endoderm
BMP	bone morphogenetic protein
Cables1	Cdk5 and Abl enzyme substrate 1
Cables2	Cdk5 and Abl enzyme substrate 2
cDNA	complementary deoxyribonucleic acid
Co-IP	co-immunoprecipitation
Ctnnb1	catenin β 1 (β-catenin)
DNA	deoxyribonucleic acid
E	embryonic day
EdU	5-ethynyl-2'-deoxyuridine
EpiLCs	epiblast-like-cells
ESCs	embryonic stem cells
GFP	green fluorescent protein
ICM	inner cell mass
WISH	whole-mount *in situ* hybridization
KOMP	Knockout Mouse Project
Luc	luciferase
mRNA	messenger ribonucleic acid
P-D	proximal - distal
PCR	polymerase chain reaction
qPCR	quantitative polymerase chain reaction

RNA	ribonucleic acid
RT-PCR	reverse transcription polymerase chain reaction
T	Brachyury
TGF-β	transforming growth factor-β
TUNEL	terminal deoxynucleotidyl transferase (TdT)-dUTP nick end labeling
VE	visceral endoderm

Contents

Abstract

CDK5 and Abl enzyme substrate 2 (Cables2), a member of the Cables family that has a C-terminal cyclin box-like domain, is widely expressed in adult mouse tissues. Forced expression of Cables2 has been shown to induce apoptotic cell death *in vitro*. However, the physiological role of Cables2 *in vivo* is unknown. Here, I showed that Cables2 plays an important role in Nodal/Smad2 and Wnt/β-catenin signalling pathways during early embryonic development in mice. *In vivo* analyses indicated that the *Cables2* gene is ubiquitously expressed in early mouse embryos and *Cables2*-deficient mice are embryonic lethal with defects of anterior visceral endoderm and primitive streak formation. In addition, I showed that Cables2 physically interacts with Smad2 and β-catenin, and enhances their transcriptional activities. Notably, *Cables2*-deficient embryos show abnormal expression of target genes of Smad2 and/or β-catenin. These results suggest that Cables2 is a Smad2 and β-catenin regulatory factor and play an essential function for mouse gastrulation. My study is the first evidence for the functional role of Cables2 *in vivo*, and may contribute to the molecular understanding of the native functions of the Cables gene family.

Introduction

At the blastocyst stage, the mouse embryo consists 2 layers: the outer trophectoderm, which will make extra-embryonic ectoderm and ectoplacental cone; and the inner cell mass (ICM), characterized as pluripotent stem cells, from which the epiblast and primitive endoderm derived. Epiblast cells will give rise to all cell types of the fetal tissues and future body, the primitive endoderm will produce the visceral endoderm (VE) lining the extraembryonic yolk sac while all extraembryonic tissues are critical to providing support for embryo development *in utero*. Following implantation, the extra- and embryonic tissues transform into the egg cylinder, a simple cylindrical structure that exhibits a molecular pattern along its proximal-distal (P-D) axis (Arnord and Robertson, 2009; Tam and Loebel, 2007). By embryonic day 5.5 (E5.5), the group of visceral endodermal cells have assembled at the distal tip of the egg cylinder, subsequently, expanded and migrated unilateral movement towards the proximal region of the egg cylinder to specify the site anterior visceral endoderm (AVE) (Beddington and Robertson, 1999; Morris et al., 2012; Varlet et al., 1997). This movement is critical for correct positioning of the anterior-posterior (A-P) axis. The primitive streak is generated initially at E6.5 from the proximal-posterior region of the epiblast and extended anteriorly to the distal tip of the egg cylinder. In mice, the formation of the primitive streak at E6.5 marks the overt morphological initiation of gastrulation stage in which three germ layers form importantly: ectoderm, mesoderm and endoderm (Tam and Loebel, 2007).

Nodal, bone morphogenetic protein (BMP), members of transforming growth factor TGF-β family, and Wnt signalling pathways are essential for early mouse

development. These signalling pathways coordinately control formation of the P-D and A-P axes during the egg cylinder stage (Shen et al., 2007; ten Berge et al., 2008; Wang et al., 2012; Winnier et al., 1995). Nodal/Smad2 signaling has the important function for establishing the AVE and hence A-P polarity of the embryo and controlling the stem cell differentiation (Brennan et al., 2001; Perea-Gomez et al., 2002; Shen et al., 2007; Yamamoto et al., 2004; Waldrip et al. 1998). It is well known that AVE formation is the result of a combination of inductive signaling by Nodal and Activin and inhibitory signals by BMP pathway. In the epiblast, Wnt3 is critically required for maintenance high levels of Nodal via regulation of the proximal enhancer in Nodal locus (Ben-Haim et al., 2006; Vincent et al., 2003). For the gastrulation, the primitive streak formation is required and preceded by the regionalized expression of lineage-specific markers such as *Brachyury* (*T)* and *Wnt3*, which are regulated by Wnt/β-catenin pathway (Rivera-Perez and Magnuson, 2005; Tam et al., 2006).

The cyclin-dependent kinase regulatory protein Cables family, abbreviated as Cables (Cdk5 and Abl enzyme substrate), has two members in mammals, designated as Cables1 and Cables2. Cables1 encodes 568 amino acid with approximate 64 kDa molecular weight and is the founding member of the Cables family. Cables1 was reported to bind to Cdk5 and c-Abl and stimulate tyrosine phosphorylation of Cdk5, which resulted in neurite outgrowth (Zukerberg et al., 2000). At the same time, *Cables1* was also isolated from the interaction with Cdk3 using the yeast two-hybrid system and being the substrate of Cdk3-mediated phosphorylation (also known as *ik3-1*) (Matsuoka et al., 2000; Yamochi et al., 2001). Of note, *Cables1*-deficient mice

showed increased cellular proliferation in endometrial hyperplasia, colon cancer, and oocyte development (Zukerberg et al., 2004; Kirley et al., 2005 and Lee et al., 2007). Furthermore, the function of Cables1 was further explored as a mediated regulator protein in the nervous system (Wu et al., 2001; Dong et al., 2003; DeBernado et al., 2005). Indeed, it has also been demonstrated that Cable1 functions as a bridging factor linking Robo-associated Abl and N-cadherin-associated β-catenin complex in chick neural retina cells (Rhee et al., 2007). Recently, *Cables1* was shown to be essential for neural differentiation in zebrafish embryos (Groeneweg et al., 2011).

Cables2 was firstly cloned by cross-hybridization with Cables1. Analysis of amino acid sequence indicated that Cables2 has the C-terminal cyclin-box-like region highly homologous to that of Cables1 (Sato et al., 2002). The Cables gene family has been found since 2000, however, most of the studies exclusively focused on Cables1 function in mouse and human tissues. Up to date, there are only two reports about Cables2 function *in vitro* which demonstrated Cables2 associates with Cdk3, Cdk5 and Abl (Sato et al., 2002), and both p53-dependent and p53-independent apoptotic pathways are related with Cables2 by cyclin box domain activity in C-terminal (Matsuoka et al., 2003).

Recently, our group found that Cables1 might contribute to the callosal formation in mouse brain. A mutated *Cables1* allele was randomly generated by transgene insertion into the genomic region containing exon 4 of *Cables1* and translated into a truncated Cables1 protein product. Notably, the *Cables1*-null mutant mice are alive with undetectable abnormal phenotype in mouse brain tissues. Generally, our study indicated that a dominant negative effect of truncated Cables1

causes the agenesis of the corpus callosum and wild-type Cables1 contributes to the callosal formation (Mizuno and Tra et al., 2014). The previous study also showed that the *Cables2* gene was expressed in a variety of adult mouse tissues, including the brain (Sato et al., 2002), thus we hypothesized the interaction of Cables2 and Cables1 in mouse brain. The effect of Cables1 dysfunction in null mutation may be masked by a redundant function of Cables2 in callosal development. In fact, no data have been reported regarding colocalization of Cables1 and Cables2 expression in the brain, neither *in vivo* function of *Cables2*, the role of *Cables2* gene should be studied and clarified to broaden our understanding of Cables1, Cables2 and Cables gene family in general.

From the lack of biological comprehension about *Cables2* gene and mutual effect between *Cables1* and *Cables2,* I aimed to analyse the role of *Cables2 in vivo* to investigate and understand the novel function of this cyclin-dependent kinase regulatory protein. To elucidate the role of Cables2 *in vivo*, I generated *Cables2-*deficient mice and found that *Cables2* deficiency caused early embryonic lethality. In addition, whole-mount *in situ* hybridization (WISH) revealed that distal visceral endoderm (DVE) and primitive streak formation were impaired in *Cables2*-deficient embryos. I further demonstrated the physical interaction of Cables2 with β-catenin and Smad2, and augmentation of their transcriptional activity by Cables2. These findings provide novel insights into the functional role of Cables2 in the regulation of Nodal/Smad2 and Wnt/β-catenin signalling during early mouse development.

Materials and Methods

Animals and husbandry

ICR mice were purchased from CLEA Japan Co. Ltd.; C57BL/6N mice were purchased from Charles River Laboratory Japan Co. Ltd. For production of staged embryos, the day of fertilization, as defined by the appearance of a vaginal plug, was considered to be embryonic day 0.5 (E0.5). Animals were kept in plastic cages (4 - 5 mice per cage) under specific pathogen-free conditions in a room maintained at 23.5°C ± 2.5°C and 52.5% ± 12.5% relative humidity under a 14-h light:10-h dark cycle. Mice had free access to commercial chow (MF; Oriental Yeast Co. Ltd.) and filtered water throughout the study. Animal experiments were carried out in a humane manner with approval from the Institutional Animal Experiment Committee of the University of Tsukuba in accordance with the Regulations for Animal Experiments of the University of Tsukuba and Fundamental Guidelines for Proper Conduct of Animal Experiment and Related Activities in Academic Research Institutions under the jurisdiction of the Ministry of Education, Culture, Sports, Science, and Technology of Japan.

Generation of *Cables2*-deficient mouse

The targeted embryonic stem cell (ESC) clone *Cables2*$^{tm1(KOMP)Vlcg}$ was purchased from KOMP (project ID VG1608, clone number: 16085A-D3).

To generate *Cables2*-deficient mice, ESCs were aggregated with the wild-type morula and transferred to pseudopregnant female mice. Male chimeras that transmitted the mutant allele to the germ line were mated with wild-type females to produce *Cables2*-deficient mice with the C57BL/6N background. Adult mice were genotyped using genomic DNA extracted from the tail. For whole-mount *in situ* hybridization, embryos were genotyped using a fragment of yolk sac and Reichert membrane. Samples were dispensed into lysis solution (50 mM Tris-HCl, pH 8.5, 1 mM EDTA, 0.5% Tween 20) and digested with proteinase K (1 mg/mL) at 55°C for 2 hours, inactivated at 95 °C for 5 minutes, and then subjected to PCR. For paraffin slides, embryos were genotyped using tissue picked from sections and digested directly with proteinase K (2 mg/mL) in PBS. For others experiments, after collecting data, the whole embryos were used for genotyping. Genotyping PCR was performed with AmpliTag Gold 360 Master Mix (Thermo Fisher Scientific) using the following primers:

> *Cables2* D3-1:   5'-ACTGCAGAAGCTGGAGGAAA-3'
>
> *Cables2* D3-2:   5'-TCAAGGTGTCTGCCCTATCC-3'
>
> *Cables2* D3-3:   5'-AGGGGATCCGCTGTAAGTCT-3'

***Nanog*-GFP reporter mice**

Nanog-GFP transgenic mice were obtained from Riken BioResource Center (BRC) (RBRC02290). Animals were kept and maintained under the same conditions as described above.

To produce the *Nanog*-GFP reporter in the homozygous *Cables2* background, *Cables2* heterozygotes were first crossed with *Nanog*$^{GFP/+}$ to obtain *Cables2*$^{+/-}$:*Nanog*$^{GFP/+}$. Subsequently, to obtain *Cables2*$^{-/-}$:*Nanog*$^{GFP/+}$ embryos, *Cables2* heterozygotes were mated with *Cables2*$^{+/-}$:*Nanog*$^{GFP/+}$ mice and the embryos were collected at E6.5 or E5.5. All embryos were then genotyped using both *Cables2* genotyping primers and the GFP following primers:

GFP F: 5'- ACGTAAACGGCCACAAGTTC-3'

GFP R: 5'- TGCTCAGGTAGTGGTTGTCG-3'

Cell culture

293FT (Thermo Fisher Scientific) cells were cultured in Dulbecco's modified Eagle's medium (DMEM) supplemented with 10% heat-inactivated fetal bovine serum. Mouse ESCs were maintained on 0.1% gelatine-coated dishes in medium consisting of DMEM containing 20% knockout serum replacement (KSR; Thermo Fisher Scientific), 1% non-essential amino acids (Thermo Fisher Scientific), 1% GlutaMAX (Thermo Fisher Scientific), 0.1 mM 2-mercaptoethanol (Thermo Fisher Scientific), and leukemia inhibitory factor (LIF)-containing conditioned medium, supplemented with two chemical inhibitors (2i), i.e., 3 μM CHIR99021 (Stemgent) and 1 μM PD0325901 (Stemgent). The epiblast-like cells (EpiLCs) were induced by plating 2.0×10^5 ESCs on human fibronectin (Corning)-coated 6-well plates in N2B27-containing NDiff 227 medium (Takara) supplemented with 20 ng/mL activin A, 12 ng/mL bFGF, and 1% KSR. All cells were cultured in an atmosphere of 5%

CO_2 at 37°C.

RT-PCR and RT-qPCR

Cultured ES cells, about 130 blastocysts, and 21 embryos at E7.5 were collected. Total RNAs from blastocysts and embryos were extracted using Isogen (Nippon Gene). RNA from ESCs was collected using an RNeasy Mini Kit (Qiagen). The cDNA was synthesized using Oligo-dT primer (Thermo Fisher Scientific) and SuperScript III Reverse Transcriptase (Thermo Fisher Scientific) in a 20-μL reaction mixture. The PCR reactions were performed with AmpliTag Gold 360 Master Mix (Thermo Fisher Scientific), *Gapdh* was used as an internal control. The primers were:

Cables1 F: 5'-CATCTTTGGAGACCCTGGAA-3'

Cables1 R: 5'-GGAAGGTCAGAACTCGCTTG-3'

Cables2 F: 5'-CACCAGCTGGCACAGAACTA-3'

Cables2 R: 5'-GCTTGAGGATCAAGTGTGGTTCAAAGTC-3'

Gapdh F: 5'-ACCACAGTCGATGCCATCAC-3'

Gapdh R: 5'-TCCACCACCCTGTTGCTGTA-3'

RT-qPCR was performed using SYBR Premix Ex Taq II (Takara) and the Thermal Cycler Dice Real Time System (Takara) according to the manufacturer's instructions. The *Nanog* gene expression level was normalized to the endogenous *Gapdh* expression level. The primers used were:

Nanog F: 5'-CCTGAGCTATAAGCAGGTTAAG-3'

Nanog R: 5'-GTGCTGAGCCCTTCTGAATC-3'

Gapdh qPCR F: 5'-TGGAGAAACCTGCCAAGTATG-3'

Gapdh qPCR R: 5'-GGAGACAACCTGGTCCTCAG-3'

Vector construction

Part of *Cables2* cDNA containing exons 1 and 2 was cloned in-frame into pBlueScript KS+ at the *Bam*HI site, and the fragment containing exons 3-10 was cloned into the pcDNA3 vector at the *Bam*HI site. These fragments were obtained and amplified from a mouse embryo E7.5 cDNA library and sequenced. The part covering *Cables2* exons 1 and 2 was cut at the *Afe*I site and ligated into the pcDNA3 vector containing exons 3-10. Finally, the full-length cDNA and FLAG-*Cables2* vectors were constructed. The full-length *Smad2* cDNA was amplified by PCR from mouse ESC cDNA template, cloned into the pcx-CAG vector, and sequenced.

A 1.5-kb *Cables2* riboprobe was prepared by amplification from the full-length cDNA template with the pcDNA3 backbone, synthesized with Sp6 polymerase, and labelled with digoxigenin as a riboprobe.

Whole-mount *in situ* hybridization (WISH)

All embryos were dissected from the decidua in PBS with 10% fetal bovine serum and staged using morphological criteria (Downs and Davies, 1993) or described as the number of days of development. WISH was carried out following standard procedures, as described previously (Rosen and Beddington, 1994). Briefly, embryos

were fixed overnight at 4°C in 4% paraformaldehyde in PBS, dehydrated, and rehydrated through a graded series of 25% - 50% - 75% methanol/PBS. After proteinase K (10 μg/mL) treatment for 15 minutes, embryos were fixed again in 0.1% glutaraldehyde/4% paraformaldehyde in PBS. Pre-hybridization at 70°C for at least 1 hour was conducted before hybridization with 1 – 2 μg/mL digoxigenin-labelled riboprobes at 70°C overnight. Pre-hybridization solution included 50% formamide, 4×SSC, 1% Tween-20, heparin (50 μg/mL) (Sigma-Aldrich) and hybridization was added more yeast RNA (100 μg/mL) and Salmon Sperm DNA (100 μg/mL) (Thermo Fisher Scientific). For post-hybridization, embryos were washed with hot solutions at 70°C including 50% formamide, 4×SSC, 1% SDS, and treated with 100 μg/mL RNase A at 37°C for 1 hour. After additional stringent hot washes at 65°C including 50% formamide, 4×SSC, samples were washed with TBST, pre-absorbed with embryo powder, and blocked in blocking solution (10% sheep serum in TBST) for 2 – 5 hours at room temperature. The embryo samples were subsequently incubated with anti-digoxigenin antibody conjugated with alkaline phosphatase anti-digoxigenin-AP, Fab fragments (Roche) overnight at 4°C. Extensive washing in TBST was followed by washing in NTMT and incubation in NBT/BCIP (Roche) at room temperature (RT) until colour development. After completion of in situ hybridization (ISH), embryos were de-stained in PBST for 24 – 48 hours and post-fixed in 4% paraformaldehyde in PBS. Embryos were processed for photography through a 50%, 80%, and 100% glycerol series. Before embedding for cryosectioning, embryos were returned to PBS and again post-fixed in 4% paraformaldehyde in PBS. The specimens were placed into OCT cryoembedding solution, flash-frozen in liquid nitrogen, and cut into sections 14

μm thick using a cryostat (HM525 NX; Thermo Fisher Scientific). The following probes were used for WISH: *Bmp4* (Jones et al., 1991), *Brachyury (T)* (Herrmann et al., 1991), *Cer1* (Belo et al., 1997), *Lim1* (Shawlot and Behringer, 1995), *Nanog* (Chambers et al., 2003) and *Wnt3* (Roelink et al., 1990).

Co-immunoprecipitation (Co-IP)

At 1 day before transfection, aliquots of 4×10^4 293FT cells were seeded onto poly-L-lysine (PLL)-coated 6-cm dishes and co-transfected with 2 μg of each pCAG-based expression vector using Lipofectamine 3000 (Thermo Fisher Scientific). After 48 hours, the cells were washed once with PBS, resuspended in RIPA buffer (50 mM Tris-HCl, pH 7.4, 150 mM NaCl, 1 mM EDTA, 1% deoxycholic acid, and 1% Nonidet P-40) containing protease inhibitor cocktail (Roche Diagnostics) and placed on ice for 30 minutes. The supernatant was collected after centrifugation and incubated with Dynabeads Protein G (Veritas) and mouse anti-DYKDDDDK (FLAG)-tag antibody (KO602-S; Transgenic) overnight at 4°C. The beads were washed four times with PBS, resuspended in Laemmli sample buffer, and boiled. The precipitated proteins were analysed by SDS-polyacrylamide gel electrophoresis (SDS-PAGE) and western blotting using the ECL Select Western Blotting Detection System (GE Healthcare) and a LAS-3000 imaging system (GE Healthcare). The FLAG antibody was then washed out and the membrane was re-stained with anti-β-catenin antibody (RCAB0001P; ReproCELL) or anti-HA High Affinity antibody (3F10; Roche).

Luciferase reporter assay

293FT cells were maintained in Dulbecco's modified Eagle's medium (DMEM) (Thermo Fisher Scientific) containing 10% fetal bovine serum (Nichirei Biosciences) and 1% penicillin-streptomycin (10000 units of penicillin and 10 mg/mL of streptomycin; Thermo Fisher Scientific) at 37°C in an atmosphere of 95% air and 5% CO_2. A total of 50,000 cells were plated in PLL-coated 96-well tissue culture plates. After overnight culture, the cells were transfected with a specific promoter-driven firefly reporter plasmid and *Renilla* luciferase control plasmid, pRL-TK, using Lipofectamine 3000 (Thermo Fisher Scientific) and opti-MEM (Thermo Fisher Scientific). Luciferase activity was analysed using a luminometer and a Dual-Glo Luciferase assay kit according to the manufacturer's instructions (Promega). The firefly luciferase values were normalized to those of *Renilla* luciferase. To evaluate β-catenin activity, cells were transiently transfected with TOPflash (TOP) or FOPflash (FOP) reporter plasmids carrying multiple copies of a wild-type or mutated TCF-binding site, respectively. Relative activity was calculated as normalized relative light units of TOPflash divided by normalized relative light units of FOPflash. To examine the SMAD2 activity, cells were transfected with ARE-luc reporter plasmid, which expresses firefly luciferase driven by a SMAD2- and FAST1-dependent promoter, pRL-TK, a FAST1 expression plasmid[48], and a constitutive-active mutant form of ALK5 expression plasmid. *Nanog* promoter activity was evaluated using the Nanog5p-luc reporter plasmid, which contains 2.5 kb of 5' promoter region of the mouse *Nanog* gene (Addgene plasmid #16337). The experiment was performed in triplicate and repeated at least three times.

Histology, EdU, and TUNEL assay

Mouse uteri including the decidua were collected and fixed in 4% paraformaldehyde in PBS. Subsequently, paraffin blocks were made by dehydration in ethanol, clearing in xylene, and embedding in paraffin. Embryo sections 5 μm thick were cut (Microm HM 335E; Thermo Fisher Scientific) and placed on glass slides (Matsunami). For haematoxylin-eosin (HE) staining, slides were deparaffinized and rehydrated through an ethanol series, and then stained with HE.

To label the proliferating embryonic cells, pregnant mice at E6.5 were injected intraperitoneally with 5-ethynyl-2'-deoxyuridine (EdU) at 200 μL/mouse and sacrificed 4 hours later. Embryos were embedded in paraffin blocks, and sections were refixed in 4% paraformaldehyde and permeabilized in 0.5% Triton X-100/PBS. EdU assay was performed with a Click-iT Plus EdU Imaging Kit (Thermo Fisher Scientific) and TUNEL assay was performed with a Click-iT Plus TUNEL Assay for In situ Apoptosis Detection kit (Thermo Fisher Scientific) according to the manufacturer's protocol. As the final step, embryo sections were co-stained with Hoechst 33342, observed under a microscope (BZ-X700; Keyence), and cell number was counted using ImageJ software.

Results

Expression of Cables gene family during early mouse development

Most of the previous studies exclusively investigated the function of *Cables1* gene in tissues and cells. Northern blotting analysis indicated that *Cables2* is widely expressed at equivalent levels in mouse tissues, including the brain, heart, muscle, thymus, spleen, kidney, liver, stomach, testis, skin, and lung (Sato et al., 2002). I first investigated the expression of *Cables* gene family in mouse embryonic stem cells (ESCs), blastocysts and embryos at day E7.5 by reverse transcription polymerase chain reaction (RT-PCR). The results indicated that both *Cables1* and *Cables2* were expressed in all three stages of development **(Fig. 1A)**.

To confirm *Cables2* gene expression in mouse embryogenesis, localization of *Cables2* mRNA expression was examined in embryos by WISH **(Fig. 1B-F)**. The data for the whole embryo and transverse section showed that *Cables2* was expressed ubiquitously at E6.5 **(Fig. 1B, C)**. *Cables2* was detected in both extra- and embryonic parts at E7.5 **(Fig. 1D)** and was strongly expressed in the allantois and heart-field at E8.5 **(Fig. 1E)**. At E9.5, the whole embryo and extraembryonic tissues, including the yolk sac, expressed *Cables2* **(Fig. 1F)**. Overall, the expression of *Cables2* is consistent with RT-PCR data, and indicates that *Cables2* is expressed ubiquitously during early development, particularly at the gastrulation stage in mouse embryo.

Early embryonic lethality of *Cables2*-deficiency

Cables2 heterozygous mice with C57BL/6N genetic background were produced successfully using conventional aggregation with *Cables2*-targeted ES cell clones obtained from KOMP. After breeding several progenies, interestingly, while the heterozygotes were viable and fertile, no homozygous *Cables2*-deficient mice were generated by intercrossing heterozygous mice **(Fig. 2A)**. In adult mice, from a total number of 90 mice, 24 were genotyped as wild-type and 66 as heterozygotes **(Table 1)**. To identify the critical point in development at which *Cables2* is essential for survival, I collected embryos at various time points during embryonic development as shown in **Table 1,** and the Mendelian ratios of *Cables2* mutant mice were determined. Homozygous *Cables2* mutant mice were detected at E6.5 – E9.5 and no homozygous embryos were found after E12.5. The genotyping PCR data showed that homozygotes were detected in embryonic stage but not in adult mice **(Fig. 2A)**.

To confirm the *Cables2* deficiency, I performed WISH using both wild-type and *Cables2*-deficient embryos at E6.5. WISH-positive staining appeared only in wild-type but not in homozygous *Cables2* mutants **(Fig. 2B)**, indicating the depletion of *Cables2* in our mouse model. The expression timeline, survival rate, and Mendelian ratio of *Cables2*-deficient embryos indicate that embryonic lethality is due to loss of *Cables2*.

Defective morphology and histology of *Cables2*-deficient embryos at the gastrulation stage

I demonstrated that in comparison with wild-type embryos, *Cables2*-deficient embryos were smaller in size and did not show the proper morphology and development at the relevant stages after E6.5. At E8.5, *Cables2*-deficient embryos were markedly smaller and showed poor development **(Fig. 3C, D)**. Wild-type embryo at E7.5 showed a well-organized structure at the neural plate stage with the allantois bud and embryonic cavities **(Fig. 3A)**. The node, headfold, and distal extension of mesoderm were observed by histological analysis **(Fig. 3G)**. However, both the extra- and embryonic regions were smaller in *Cables2*-deficiency, which could be clearly distinguished from other embryos in the same litter at E7.5 **(Fig. 3B, H)**.

The *Cables2*-deficient embryos at E6.5 showed the unclear abnormal phenotype histologically compared with the others **(Fig. 3E, F)**. These data suggest that homozygous *Cables2* mutants have disrupted development for gastrulation.

Normal cell proliferation and death status in *Cables2*-deficient embryos

Cell proliferation and apoptotic cell death are key events during development. To clarify the cell growth status, I performed EdU assay and measured the percentage of EdU-positive cells. The numbers of cells were counted in at least 2 slides per sample. There was no significant difference in the number of proliferation cells between wild-type and *Cables2*-deficient embryos at E6.5 **(Fig. 4A, B, G)**.

Furthermore, TUNEL assay was performed simultaneously to determine whether the embryonic lethality observed in *Cables2*-deficient embryos was related to

programmed cell death. Although apoptotic cells were detected in both epiblast and embryo visceral endoderm, the average percentage of dead cells in *Cables2*-deficient embryos was similar to that in wild-type embryos **(Fig. 4C-F, H)**. Those results suggested that cell proliferation and apoptotic cell death are not the main causes of *Cables2* embryo lethality.

Impaired A-P axis specification and primitive streak formation in *Cables2*-deficiency

To understand the mechanisms underlying the defects in *Cables2*-deficient embryos, I first analysed the expression of several markers of gastrulation and primitive streak formation. *Brachyury (T)* is expressed in the posterior–distal axis of the streak and is a commonly used marker of gastrulation (Wilkinson et al., 1990). As the result, *T* was expressed in the primitive streak and node of wild-type embryos at E7.5 **(Fig. 5E)**. At this stage, *Cables2*-deficient embryo had just formed the primitive streak and mesodermal cells started migrating toward the distal **(Fig. 5F)**. At E6.5, *Cables2*-deficient embryos exhibited spatial and quantitative impairment of *T* expression compared with wild-type embryos **(Fig. 5C, D).** *Wnt3*, a critical marker for gastrulation and Wnt/β-catenin signalling in the embryo, also showed impaired expression throughout the proximal epiblast in *Cables2* mutants **(Fig. 5A, B)**. These results suggest that *Cables2* is required for the proper formation of primitive streak. The P-D and A-P axes are primary and critical developmental steps to initiate gastrulation and achieve correct embryo patterning. *Bmp4*, a P-D axis marker, showed similar expression in the extraembryonic tissues of both wild-type and *Cables2*-

deficiency **(Fig. 5G, H)**, suggesting that P-D specification is normal in E6.5 embryos lacking *Cables2*. Prior to gastrulation, the DVE migrates to the prospective anterior side for correct positioning of the anterior visceral endoderm (AVE). The A–P polarity is formed from this process and mostly regulated by Nodal signalling (Takaoka and Hamada, 2012). Therefore, I next examined the AVE and A-P axis formation in embryos. *Lim1*, which is normally expressed in the lateral mesoderm and anterior endoderm of wild-type embryos (Shawlot and Behringer, 1995), was accumulated in the distal part of *Cables2*-deficient E6.5 embryos **(Fig. 5I, J)**. *Cer1*, an antagonist of Nodal signaling, is expressed distally and anteriorly in the visceral endoderm and restricted to the anterior end at E6.0 (Belo et al., 1997). My data showed that *Cer1* was mislocalized and expressed at lower levels in *Cables2*-deficient embryos compared to the wild-type at E6.5 **(Fig. 5K, L)**. Taken together, the results of WISH analyses indicate that *Cables2* depletion impairs the correct AVE localization and leads to defective primitive streak formation at the gastrulation stage.

Activation and interaction of Cables2 with β-catenin *in vitro*

Wnt signalling is a fundamental pathway to maintain and specify patterning during embryogenesis (Tam PP and Loebel DA, 2007). As the Wnt/β-catenin markers, *T* and *Wnt3*, showed impaired expression in *Cables2*-null mutant embryos **(Fig. 5A-F)**, I examined whether Cables2 facilitates β-catenin activity *in vitro* by TOP/FOP reporter assay. 293FT cells were transfected with Wnt reporter plasmids and assayed for the β-catenin/TCF-mediated luciferase activity. The results indicated that Cables2 activated β-catenin/TCF-mediated transcription in 293FT cells, with an almost two-

fold increase in relative TOP/FOP activity **(Fig. 6A)**. This result suggests that Cables2 activates Wnt/β-catenin signaling.

To further investigate the interaction of Cables2 and β-catenin, I perform the Co-IP using FLAG-Cables2 and β-catenin transfected 293FT cell lysates. After washing out the FLAG antibody, β-catenin was present in the precipitated complexes with Cables2 **(Fig. 6B).** These data suggest that Cables2 activated and was physically associated with β-catenin *in vitro*.

Activation and interaction of Cables2 with Smad2 *in vitro*

Nodal/Smad2 signalling is one of the essential factors for primitive streak formation. Previous studies have shown that Smad2/3 and Oct4 function together with β-catenin in inducing primitive streak genes including *T* (Funa et al., 2015). Therefore, I investigated the functional relations between Cables2 and Smad2. Luciferase reporter assay with the ARE-luc vector, which expresses firefly luciferase in a Smad2- and FAST1-dependent manner, indicated that forced expression of Cables2 facilitated Smad2 activity in 293FT cells **(Fig. 7A)**. In addition, I found that Cables2 physically interacted with Smad2 **(Fig. 7B)**. These results suggest that Cables2 is a positive regulatory factor of Smad2.

Facilitation of *Nanog* expression and its promoter activity by *Cables2*

Loss of *Cables2* caused disruption of mouse gastrulation. Therefore, I established *Cables2*-deficient ESCs from homozygous embryos at E3.5 and induced

their differentiation into epiblast-like cells (EpiLCs) to further investigate the function of *Cables2 in vitro*. The morphology, proliferation, and expression of pluripotency genes were almost identical between wild-type and *Cables2*-deficient ESCs. Both types of ESCs exhibited similar morphological changes after EpiLC induction with activin and bFGF.

Nanog plays a crucial role in early mouse embryonic development. The expression of *Nanog* has been observed in the cells of the inner cell mass (ICM) of the E3.5 blastocyst and the epiblast in the egg cylinder into the primitive streak stage (Chambers et al., 2003, Hatano et al., 2005). The cytokine dependency of Nanog expression is known to switch from LIF/Stat in ICM to Nodal/Smad2 in the epiblast. Next, I analysed the expression level and promoter activity of *Nanog* in EpiLCs lacking *Cables2* to verify whether *Cables2* regulates *Nanog* expression in epiblasts. Interestingly, quantitative RT-PCR showed that *Nanog* mRNA level was decreased by approximately 40% in *Cables2*-deficient EpiLCs **(Fig. 8A)**. Moreover, luciferase assay demonstrated that *Cables2* deficit reduced *Nanog* promoter activity in EpiLCs **(Fig. 8B)**.

Previous studies have addressed *Nanog* expression in mouse embryos at early embryonic stages by immunostaining and WISH. The data indicated that *Nanog* is expressed in the whole region of E5.5 epiblasts, but only in the posterior region of E6.5 and E7.5 epiblasts (Hart et al., 2004; Hatano et al., 2005). Consistent with these previous reports, my WISH data showed that *Nanog* was expressed in the posterior region of wild-type embryos at E6.5 **(Fig. 9E)**. In contrast, *Cables2*-deficient embryos showed only a low level of *Nanog* gene expression over the whole epiblast region at

E6.5 **(Fig. 9F)**. To confirm the expression pattern of Nanog in the E6.5 embryo, I utilized *Nanog*-GFP transgenic mice (Okita et al., 2007). Mice carrying the *Nanog*-GFP reporter were crossed with *Cables2*-deficient heterozygotes to obtain *Cables2* homozygous reporter embryos. At E6.5, *Cables2*-deficient embryos carrying *Nanog*-GFP showed even expression of Nanog in the whole epiblast and reduced GFP expression **(Fig. 9C, D)**. Nevertheless, there was no difference in GFP expression between embryos of the same litter at E5.5 **(Fig. 9A, B)**, suggesting no detectable phenotype of *Nanog* before primitive streak formation. Overall, loss of *Cables2* leads to downregulated expression of *Nanog* at the gastrulation stage.

Discussion

In this study, I demonstrated that *Cables2* was expressed ubiquitously during early embryonic development and that disruption of the *Cables2* gene caused embryonic lethality in mice. The resulting impaired A-P axis specification led to defective primitive streak formation at E6.5. Interestingly, *Wnt3* and *T*, targets of Wnt/β-catenin signalling in gastrulation, showed impaired expression in *Cables2*-deficient embryos. Moreover, Cables2 interacted with β-catenin and stimulated β-catenin/TCF-mediated transcription *in vitro*. My data further indicated that Cables2 was associated with Smad2 and activated the Smad2 reporter signal in 293T cells. In transgenic *Nanog*-GFP reporter mice, *Nanog*-positive cells appeared evenly in the epiblast and were expressed weakly in the proximal–posterior region from gastrulation. These results strongly suggested that both Wnt/β-catenin and Nodal/Smad2 signalling pathways are positively mediated by Cables2 during gastrulation **(Fig. 10)**. Taken together, the lethality in mouse embryos at the gastrulation stage associated with *Cables2* deficit indicates an essential function of *Cables2* in early mouse development.

Wnt/β-catenin-dependent pathway involving Cables2

Wnt3, Nodal, and BMP4 are key signalling molecules that control temporal and spatial development in the early stages, as well as primitive streak formation (Tam and Loebel, 2007). My data indicated that *Cables2*-deficiency caused no detectable dysfunction of BMP4, as *Bmp4* expression pattern and level were normal on WISH analysis in *Cables2*-deficient embryos. Nevertheless, it is possible that the

dysfunction of Wnt3, β-catenin, or T, downstream molecules of BMP4, occurred in *Cables2*-null mutant mice. *Wnt3* knockout embryos fail to form the primitive streak and gastrulation (Liu et al., 1999). However, AVE markers were localized correctly in *Wnt3*-deficient embryos, suggesting the dispensable or downstream function of *Wnt3* to the earlier A–P specification signals. *T*-deficient mice show morphological abnormalities in PS, notochord, neural tube, and allantois, and die at about E10.5 (Gluecksohn-Schoenheimer, 1944; Wilkinson et al., 1990). The phenotypes of *Wnt3* and *T* depletion, therefore, are different from the *Cables2* knockout model in which A-P formation was impaired. It seems that the developmental disruption of *Cables2*-deficient mice occurred at an early stage, prior to the completion of AVE migration. β-catenin is required for differentiation of germ layers and axis formation. Disruption of *Ctnnb1* (β-catenin) led to embryonic lethality; germ layers were not formed and the prospective AVE was mislocalized, as *T* was not detectable and *Cer1* and *Lim1* markers were expressed in the distal tip but not in the AVE (Huelsken et al., 2000). This AVE defect was similar to that seen in *Cables2* mutant embryos, but *Ctnnb1*-deficient embryos showed more severe abnormality as there were no signs of gastrula formation.

Generally, components of the Wnt signalling pathway act as the key factors for at least two processes during early development, i.e., establishment of the A-P axis and formation of the PS, the initial step in gastrulation. Several recent studies indicated that Wnt ligands play roles mostly from the stage of gastrulation, while axis specification prior to gastrula formation is mediated by β-catenin independent of Wnt (Muñoz-Descalzo et al., 2015). The phenotype of embryos lacking *Cables2* mimicked

the delayed initiation of gastrulation of the conditional inactivation of *Wnt3* in the epiblast or visceral endoderm, which showed the weak expression of *T* in the epiblast and extraembryonic ectoderm (Tortelote et al., 2013; Yoon et al., 2015). Meanwhile, the mislocalization of anterior markers is similar to *Ctnnb1*-null mutation, even though gastrulation occurred in *Cables2*-deficient embryos. My data demonstrated the novel interaction of Cables2 with β-catenin and increased β-catenin activity in 293FT cells, suggesting that *Cables2* disruption leads to β-catenin hypofunction. Thus, *Cables2*-deficiency appears to cause the primitive streak defect by dysfunction of Wnt3 and β-catenin. In fact, *T* and *Wnt3*, direct targets of β-catenin, were repressed and markedly decreased in the epiblast during gastrulation in *Cables2*-deficient embryos, respectively, but they were not completely disrupted, suggesting that β-catenin activity remained at low levels. Thus, both processes driven by β-catenin and the Wnt pathway at gastrulation stage may be affected by the lack of *Cables2*. However, the downregulated expression of the pluripotency marker, *Nanog*, in *Cables2* mutant cannot be fully explained by Wnt/β-catenin activity. It seems that additional signalling is involved in the gastrulation defect leading to embryonic lethality in *Cables2*-deficient mice.

Nodal/Smad2-dependent pathway involving Cables2

Nodal/Smad2 signalling and Oct4 have been shown to be required for *Nanog* expression, and Smad2 is an upstream regulator of *Nanog* transcription in the epiblast and primitive streak (Xu et al., 2008; Sun et al., 2014). Notably, I found that Cables2

physically interacted with Smad2 and enhanced its activity in 293FT cells. Moreover, the results of the present study clearly indicated that *Nanog* expression was dysregulated in EpiLCs and epiblasts lacking *Cables2*. These data strongly supported the possible involvement of Cables2 in Nodal/Smad2 signalling during early embryonic development. Taken together, these observations suggest that Cables2 positively regulates the Nodal/Smad2 signalling pathway in mouse embryogenesis.

Previous studies indicated that either *Smad2*- or *Nodal*-deficient embryos failed to form the proper egg cylinder and germ layers. *Nodal* plays an important role first in specification of the P-D axis by promoting the posterior cell fates and maintaining the molecular pattern in the adjacent extraembryonic ectoderm (Conlon et al., 1994; Nomura and Li, 1998, Waldrip et al., 1998; Weinstein et al., 1998). Subsequently, Smad2 is involved in the Nodal signalling cascade to regulate and pattern the visceral endoderm AVE cell migration (Brennan et al., 2001). *Nodal*-depleted embryos lack the AVE markers, *Cer1* and *Lim1*, as well as indicators of gastrulation stage, *Wnt3* and *T*. Interestingly, two of these Nodal target genes (*Cer1* and *Lim1*) were also not present, but other markers, *T* and *Wnt3*, showed high levels of ectopic expression throughout the epiblast in *Smad2*-deficient mouse embryos because of the lack of Nodal and Wnt antagonists in the anterior region. In the case of *Cables2* depletion, WISH indicated that the levels of the Nodal antagonists, *Cer1*, and the AVE marker, *Lim1*, were decreased in the anterior region. However, *Wnt3* and *T* were also repressed, probably by downregulation of Wnt/β-catenin signalling activity. Therefore, the phenotype of *Cables2*-deficiency probably resulted from dysregulation of both Nodal/Smad2 and Wnt3/β-catenin signalling. The functional role of Cables2

during gastrulation may be to cooperatively induce target gene expression via physical interactions with two key molecules, β-catenin and Smad2 **(Fig. 10)**. The abnormal development of *Cables2*-deficient embryos may be caused by the insufficient activation of both Smad2 and β-catenin, which are necessary to control AVE cell migration and both *Nanog* and *T* expression in the posterior region of the epiblast at E6.5. Consistent with this hypothesis, β-catenin and Smad2 showed collaborative interactions and specific functions for inducing primitive streak cell lineages (Funa et al., 2015). Taken together, I propose that Cables2 may function as a cofactor required for proper activation of Wnt3/β-catenin and Nodal/Smad2 signalling to maintain epiblast pluripotency, AVE formation, and primitive streak induction **(Fig. 10)**.

Requirement of Cables2 function for gastrula formation

My current data demonstrated that β-catenin activity is positively regulated by Cables2 in the epiblast of gastrula. Similarly, Cables1 and β-catenin were found having direct and essential interaction in neuronal chicken cells. Rhee and colleagues reported that Cables1 is involved in activation of β-catenin activity as a linker protein between Slit/Robo-associated Abl and N-cadherin-associated β-catenin (Rhee et al., 2007). Importantly and recently, Cables1 was explored as a tumor suppressor gene and demonstrated that in colon cancer cells, human CABLES1 deficiency increased β-catenin-dependent transcription (Arnason et al, 2013). The discrepancy implies that effect of Cables1 on β-catenin activity is dependent on cell types.

Cables1 was already expressed in mouse embryos at the blastocysts stage, but its localization was not investigated in this study. By Northern blots analysis, *Cables1* was detected in various mouse tissues, heart, brain, spleen, lung, liver, muscle, kidney and testis with the highest expression in the brain (Zukerberg et al., 2000). Although the *Cables1* expression was evident during early mouse embryo and ubiquitous manner same as *Cables2*, *Cables1*-knockout mice are viable. In this study, I showed that *Cables2*-deficient mouse embryos could not go through the gastrulation stage, despite the presence of *Cables1*. These results suggest that *Cables2* has an essential or indispensable function in gastrula.

The homology structures with 78% similarity between Cables1 and Cables2 is mainly the C-terminal which containing the cyclin domain. Their N-terminal and middle parts were reported to have six SH3 domain-binding motifs (PXXP) which regulate the Abl kinase activity (Sato et al., 2002). Besides, their N-terminal regions are non-homologous and have not been considered to maintain any important domain or effective site in amino acid sequences yet. Those parts of protein structure should be analyzed more to achieve the interaction with unknown molecules from which leading to different function between Cables1 and Cables2.

In near future, the effect of Cables2/Cables1 on β-catenin and Smad2 activation in EpiLCs or epiblast stem cells should be investigated further. Moreover, the molecular mechanisms of how β-catenin and Smad2 molecules are positively regulated by Cables2 should be disclosed.

In conclusion, Cables2 plays an essential role in mouse embryogenesis, and targeted disruption of *Cables2* leads to embryo lethality. My results strongly suggest

that *Cables2* has indispensable functions, and further investigations are required to gain a greater understanding of *Cables2* and its molecular interactions. It is notable that Cables2 was related to Wnt3/β-catenin and Nodal/Smad2 signalling during development via its interactions with β-catenin and Smad2. This study represents the first evidence for a functional role of Cables2 *in vivo*, and may contribute to the molecular understanding of the native functions of the Cables gene family.

Acknowledgements

Firstly, I would like to express my sincere gratitude to my supervisors, Prof. Fumihiro Sugiyama, Prof. Ken-ichi Yagami and Prof. Mitsuyasu Kato for giving me the opportunity to work on Laboratory of Animal Sciences and Laboratory Animal Resource Center, for the patience, motivation, enthusiasm and immense knowledge. Specially, Prof. Sugiyama inspired me in researching and writing this thesis all the time with his guidance and kindness. Together with their outstanding knowledge, their patience and enthusiasm helped so much on my work.

I would like to express my gratitude to Dr. Seiya Mizuno for giving helpful suggestions and fruitful discussion all the time. My gratitude especially goes to Dr. Hiroyoshi Iseki for supporting me in skills and data analysis.

Secondly, I am exceedingly grateful to all members in the Laboratory of Animal Sciences and all the staffs of Laboratory Animal Resource Center of Tsukuba University. My life and my study in Japan has been a wonderful and convenient time with their considerable help and great encouragement.

Besides, I would like to acknowledge Prof. Tomoki Chiba, Dr. Koichiro Kako, Dr. Yukihiro Yada and Dr. Seiya Mizuno for their contributions as members of my thesis committee and for giving me many insightful comments.

I sincerely appreciate Prof. Val Wilson, Edinburgh University and Assoc. Prof Ruth Arkell, The Australian National University for their kindness and spending the time to my International Research Rotation. The *in situ* hybridization probes were gifts from Prof. Wilson (*Brachyury, Cer1, BMP4, Nanog*) and Assoc. Arkell (*Lim1,*

References

Arnason T, Pino MS, Yilmaz O, Kirley SD, Rueda BR, Chung DC, Zukerberg LR. Cables1 is a tumor suppressor gene that regulates intestinal tumor progression in Apc(Min) mice. Cancer Biol Ther. 2013;14:672-678.

Arnold SJ, Robertson EJ. Making a commitment: cell lineage allocation and axis patterning in the early mouse embryo. Nat Rev Mol Cell Biol. 2009;10:91-103.

Beddington RS, Robertson EJ. Axis development and early asymmetry in mammals. Cell. 1999;96:195-209.

Belo JA, Bouwmeester T, Leyns L, Kertesz N, Gallo M, Follettie M, De Robertis EM. Cerberus-like is a secreted factor with neutralizing activity expressed in the anterior primitive endoderm of the mouse gastrula. Mech Dev. 1997;68:45-57.

Ben-Haim N, Lu C, Guzman-Ayala M, Pescatore L, Mesnard D, Bischofberger M, Naef F, Robertson EJ, Constam DB. The nodal precursor acting via activin receptors induces mesoderm by maintaining a source of its convertases and BMP4. Dev Cell. 2006;11:313-323.

Brennan J, Lu CC, Norris DP, Rodriguez TA, Beddington RS, Robertson EJ. Nodal signalling in the epiblast patterns the early mouse embryo. Nature. 2001;411:965-969.

Chambers I, Colby D, Robertson M, Nichols J, Lee S, Tweedie S, Smith A. Functional expression cloning of Nanog, a pluripotency sustaining factor in embryonic stem cells. Cell. 2003;113:643-655.

Conlon FL, Lyons KM, Takaesu N, Barth KS, Kispert A, Herrmann B, Robertson EJ. A primary requirement for nodal in the formation and maintenance of the primitive streak in the mouse. Development. 1994;120:1919-1928.

DeBernardo RL, Littell RD, Luo H, Duska LR, Oliva E, Kirley SD, Lynch MP, Zukerberg LR, Rueda BR. Defining the extent of cables loss in endometrial cancer subtypes and its effectiveness as an inhibitor of cell proliferation in malignant endometrial cells in vitro and in vivo. Cancer Biol Ther. 2005;4:103-107.

Dong Q, Kirley S, Rueda B, Zhao C, Zukerberg L, Oliva E. Loss of cables, a novel gene on chromosome 18q, in ovarian cancer. Mod Pathol. 2003;16:863-868.

Downs KM, Davies T. Staging of gastrulating mouse embryos by morphological landmarks in the dissecting microscope. Development. 1993;118:1255-1266.

Funa NS, Schachter KA, Lerdrup M, Ekberg J, Hess K, Dietrich N, Honoré C, Hansen K, Semb H. β-Catenin Regulates Primitive Streak Induction through Collaborative Interactions with SMAD2/SMAD3 and OCT4. Cell Stem Cell. 2015;16:639-652.

Gluecksohn-Schoenheimer S. The Development of Normal and Homozygous Brachy (T/T) Mouse Embryos in the Extraembryonic Coelom of the Chick. Proc Natl Acad Sci U S A. 1944;30:134-140.

Groeneweg JW, White YA, Kokel D, Peterson RT, Zukerberg LR, Berin I, Rueda BR, Wood AW. cables1 is required for embryonic neural development: molecular, cellular, and behavioral evidence from the zebrafish. Mol Reprod Dev. 2011;78:22-32.

Hart AH, Hartley L, Ibrahim M, Robb L. Identification, cloning and expression analysis of the pluripotency promoting Nanog genes in mouse and human. Dev Dyn. 2004;230:187-198.

Hatano SY, Tada M, Kimura H, Yamaguchi S, Kono T, Nakano T, Suemori H, Nakatsuji N, Tada T. Pluripotential competence of cells associated with Nanog activity. Mech Dev. 2005;122:67-79.

Hayashi H, Abdollah S, Qiu Y, Cai J, Xu YY, Grinnell BW, Richardson MA, Topper JN, Gimbrone MA Jr, Wrana JL, Falb D. The MAD-related protein Smad7 associates with the TGFbeta receptor and functions as an antagonist of TGFbeta signaling. Cell. 1997;89:1165-1173.

Herrmann BG. Expression pattern of the Brachyury gene in whole-mount TWis/TWis mutant embryos. Development. 1991;113:913-917.

Huelsken J, Vogel R, Brinkmann V, Erdmann B, Birchmeier C, Birchmeier W. Requirement for beta-catenin in anterior-posterior axis formation in mice. J Cell Biol. 2000;148:567-578.

Jones CM, Lyons KM, Hogan BL. Involvement of Bone Morphogenetic Protein-4 (BMP-4) and Vgr-1 in morphogenesis and neurogenesis in the mouse. Development. 1991;111:531-542.

Kirley SD, D'Apuzzo M, Lauwers GY, Graeme-Cook F, Chung DC, Zukerberg LR. The Cables gene on chromosome 18Q regulates colon cancer progression in vivo. Cancer Biol Ther. 2005;4:861-863.

Lee HJ, Sakamoto H, Luo H, Skaznik-Wikiel ME, Friel AM, Niikura T, Tilly JC, Niikura Y, Klein R, Styer AK, Zukerberg LR, Tilly JL, Rueda BR. Loss of CABLES1, a cyclin-dependent kinase-interacting protein that inhibits cell cycle progression, results in germline expansion at the expense of oocyte quality in adult female mice. Cell Cycle. 2007;6:2678-2684.

Liu P, Wakamiya M, Shea MJ, Albrecht U, Behringer RR, Bradley A. Requirement for Wnt3 in vertebrate axis formation. Nat Genet. 1999;22:361-365.

Matsuoka M, Matsuura Y, Semba K, Nishimoto I. Molecular cloning of a cyclin-like protein associated with cyclin-dependent kinase 3 (cdk 3) in vivo. Biochem Biophys Res Commun. 2000;273:442-447.

Matsuoka M, Sudo H, Tsuji K, Sato H, Kurita M, Suzuki H, Nishimoto I, Ogata E. ik3-2, a relative to ik3-1/Cables, is involved in both p53-mediated and p53-independent apoptotic pathways. Biochem Biophys Res Commun. 2003;312:520-529.

Mizuno S, Tra DT, Mizobuchi A, Iseki H, Mizuno-Iijima S, Kim JD, Ishida J, Matsuda Y, Kunita S, Fukamizu A, Sugiyama F, Yagami K. Truncated Cables1 causes agenesis of the corpus callosum in mice. Lab Invest. 2014;94:321-330.

Morris SA, Grewal S, Barrios F, Patankar SN, Strauss B, Buttery L, Alexander M, Shakesheff KM, Zernicka-Goetz M. Dynamics of anterior-posterior axis formation in the developing mouse embryo. Nat Commun. 2012;3:673.

Muñoz-Descalzo S, Hadjantonakis AK, Arias AM. Wnt/ß-catenin signalling and the dynamics of fate decisions in early mouse embryos and embryonic stem (ES) cells. Semin Cell Dev Biol. 2015;47-48:101-109.

Nomura M, Li E. Smad2 role in mesoderm formation, left-right patterning and craniofacial development. Nature. 1998;393:786-790.

Okita K, Ichisaka T, Yamanaka S. Generation of germline-competent induced pluripotent stem cells. Nature. 2007;448:313-317.

Pauklin S, Vallier L. Activin/Nodal signalling in stem cells. Development. 2015;142:607-619.

Perea-Gomez A, Vella FD, Shawlot W, Oulad-Abdelghani M, Chazaud C, Meno C, Pfister V, Chen L, Robertson E, Hamada H, Behringer RR, Ang SL. Nodal antagonists in the anterior visceral endoderm prevent the formation of multiple primitive streaks. Dev Cell. 2002;3:745-756.

Rhee J, Buchan T, Zukerberg L, Lilien J, Balsamo J. Cables links Robo-bound Abl kinase to N-cadherin-bound beta-catenin to mediate Slit-induced modulation of adhesion and transcription. Nat Cell Biol. 2007;9:883-892.

Rivera-Pérez JA, Magnuson T. Primitive streak formation in mice is preceded by localized activation of Brachyury and Wnt3. Dev Biol. 2005;288:363-371.

Roelink H, Wagenaar E, Lopes da Silva S, Nusse R. Wnt-3, a gene activated by proviral insertion in mouse mammary tumors, is homologous to int-1/Wnt-1 and is normally expressed in mouse embryos and adult brain. Proc Natl Acad Sci U S A. 1990;87:4519-4523.

Rosen B, Beddington R. Detection of mRNA in whole mounts of mouse embryos using digoxigenin riboprobes. Methods Mol Biol. 1994;28:201-208.

Sato H, Nishimoto I, Matsuoka M. ik3-2, a relative to ik3-1/cables, is associated with cdk3, cdk5, and c-abl. Biochim Biophys Acta. 2002;1574:157-163.

Shawlot W, Behringer RR. Requirement for Lim1 in head-organizer function. Nature. 1995;374:425-430.

Shen MM. Nodal signaling: developmental roles and regulation. Development. 2007;134:1023-1034.

Sun LT, Yamaguchi S, Hirano K, Ichisaka T, Kuroda T, Tada T. Nanog co-regulated by Nodal/Smad2 and Oct4 is required for pluripotency in developing mouse epiblast. Dev Biol. 2014;392:182-192.

Takaoka K, Hamada H. Cell fate decisions and axis determination in the early mouse embryo. Development. 2012;139:3-14.

Tam PP, Loebel DA, Tanaka SS. Building the mouse gastrula: signals, asymmetry and lineages. Curr Opin Genet Dev. 2006;16:419-425.

Tam PP, Loebel DA. Gene function in mouse embryogenesis: get set for gastrulation. Nat Rev Genet. 2007;8:368-381.

ten Berge D, Koole W, Fuerer C, Fish M, Eroglu E, Nusse R. Wnt signaling mediates self-organization and axis formation in embryoid bodies. Cell Stem Cell. 2008;3:508-518.

Tortelote GG, Hernández-Hernández JM, Quaresma AJ, Nickerson JA, Imbalzano AN, Rivera-Pérez JA. Wnt3 function in the epiblast is required for the maintenance but not the initiation of gastrulation in mice. Dev Biol. 2013;374:164-173.

Vincent SD, Dunn NR, Hayashi S, Norris DP, Robertson EJ. Cell fate decisions within the mouse organizer are governed by graded Nodal signals. Genes Dev. 2003;17:1646-1662.

Waldrip WR, Bikoff EK, Hoodless PA, Wrana JL, Robertson EJ. Smad2 signaling in extraembryonic tissues determines anterior-posterior polarity of the early mouse embryo. Cell. 1998;92:797-808.

Wang J, Sinha T, Wynshaw-Boris A. Wnt signaling in mammalian development: lessons from mousegenetics. Cold Spring Harb Perspect Biol. 2012, 4:a007963

Weinstein M, Yang X, Li C, Xu X, Gotay J, Deng CX. Failure of egg cylinder elongation and mesoderm induction in mouse embryos lacking the tumor suppressor smad2. Proc Natl Acad Sci U S A. 1998;95:9378-9383.

Wilkinson DG, Bhatt S, Herrmann BG. Expression pattern of the mouse T gene and its role in mesoderm formation. Nature. 1990;343:657-659.

Winnier G, Blessing M, Labosky PA, Hogan BL. Bone morphogenetic protein-4 is required for mesoderm formation and patterning in the mouse. Genes Dev. 1995;9:2105-2116.

Wu CL, Kirley SD, Xiao H, Chuang Y, Chung DC, Zukerberg LR. Cables enhances cdk2 tyrosine 15 phosphorylation by Wee1, inhibits cell growth, and is lost in many human colon and squamous cancers. Cancer Res. 2001;61:7325-7332.

Xu RH, Sampsell-Barron TL, Gu F, Root S, Peck RM, Pan G, Yu J, Antosiewicz-Bourget J, Tian S, Stewart R, Thomson JA. NANOG is a direct target of TGFbeta/activin-mediated SMAD signaling in human ESCs. Cell Stem Cell. 2008;3:196-206.

Yamamoto M, Saijoh Y, Perea-Gomez A, Shawlot W, Behringer RR, Ang SL, Hamada H, Meno C. Nodal antagonists regulate formation of the anteroposterior axis of the mouse embryo. Nature. 2004;428:387-392.

Yamochi T, Semba K, Tsuji K, Mizumoto K, Sato H, Matsuura Y, Nishimoto I, Matsuoka M. ik3-1/Cables is a substrate for cyclin-dependent kinase 3 (cdk 3). Eur J Biochem. 2001;268:6076-6082.

Yoon Y, Huang T, Tortelote GG, Wakamiya M, Hadjantonakis AK, Behringer RR, Rivera-Pérez JA. Extra-embryonic Wnt3 regulates the establishment of the primitive streak in mice. Dev Biol. 2015;403:80-88.

Zukerberg LR, DeBernardo RL, Kirley SD, D'Apuzzo M, Lynch MP, Littell RD, Duska LR, Boring L, Rueda BR. Loss of cables, a cyclin-dependent kinase regulatory protein, is associated with the development of endometrial hyperplasia and endometrial cancer. Cancer Res. 2004;64:202-208.

Zukerberg LR, Patrick GN, Nikolic M, Humbert S, Wu CL, Lanier LM, Gertler FB, Vidal M, Van Etten RA, Tsai LH. Cables links Cdk5 and c-Abl and facilitates Cdk5 tyrosine phosphorylation, kinase upregulation, and neurite outgrowth. Neuron. 2000;26:633-646.

Table 1. Survival rate and Mendelian ratio of *Cables2*-mutant embryos

Embryonic days (E)	Total number of embryos	Genotypes		
		+/+	+/-	-/-
E6.5	437	132 (30.2%)*	221 (50.6)	80 (18.3)
E7.5	70	18 (25.7)	32 (45.7)	20** (28.6)
E8.5	21	9 (42.9)	9 (42.9)	3** (14.3)
E9.5	18	7 (38.9)	7 (38.9)	4** (22.2)
E12.5	6	2 (33.3)	4 (66.7)	0 (0)
Adult	90	24 (26.7)	66 (73.3)	0 (0)

*:   Number of embryos (percentage)
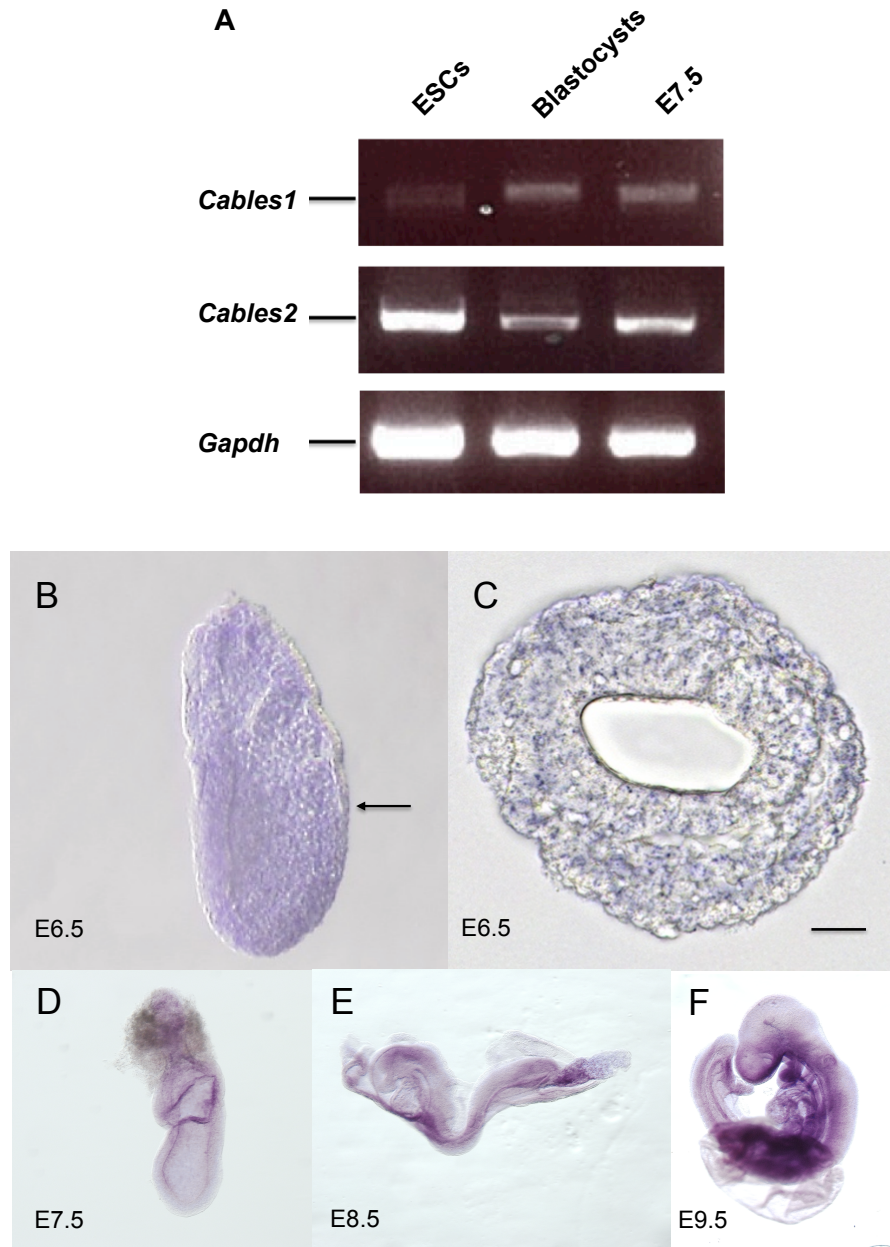
**: Abnormal phenotype

Figure 1. *Cables2* expression during early mouse embryo development

A. *Cables1* and *Cables2* gene expression were examined by RT-PCR with ESC, blastocyst and E7.5 embryo samples. *Gapdh* was used as an internal-positive control. **B-F.** Wild-type embryos from E6.5 to E9.5 were examined by WISH with *Cables2* probe. Whole embryo was expressed *Cables2* at E6.5 **(B)**. The black arrow indicates the position of transverse section shown in **(C)**. Scale bar, 20 μm.
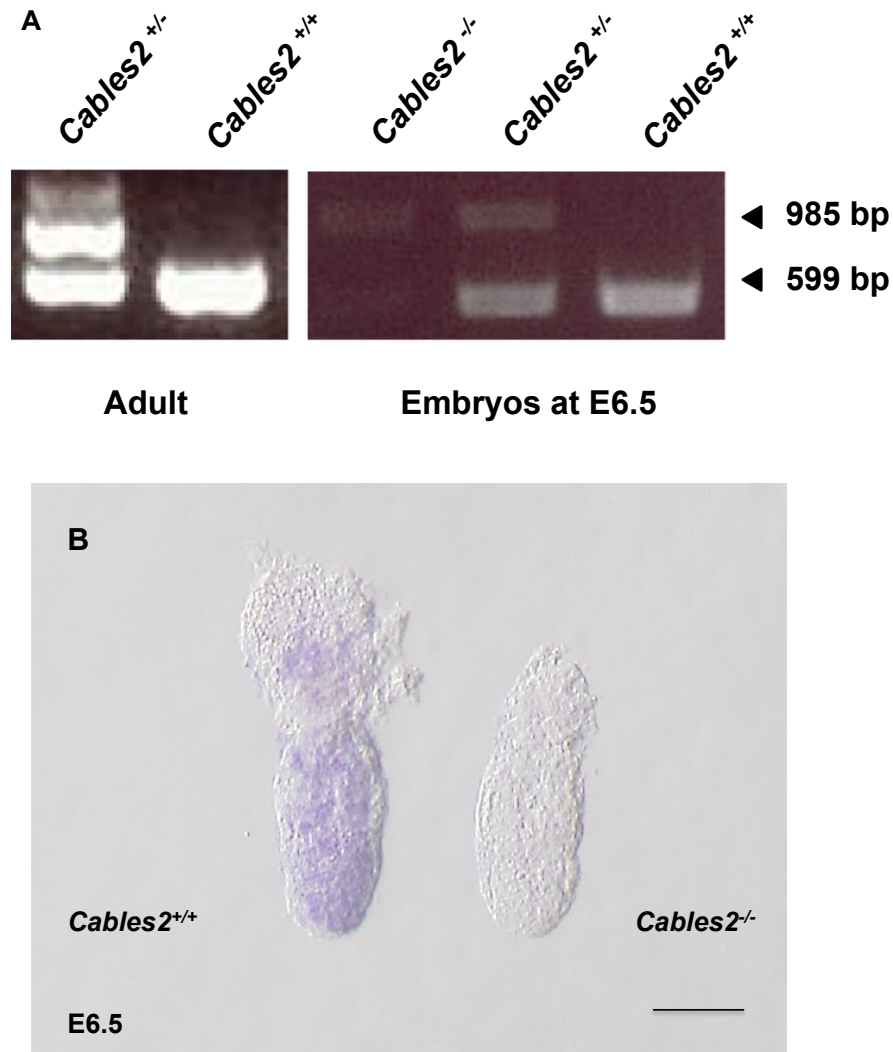
Figure 2. Genotyping and expression of *Cables2*

A. Adults and embryos were genotyped by PCR analysis from the mouse tail or whole embryo samples using three primers. Bands at 985 bp and 599 bp represent mutant and wild-type *Cables2* alleles, respectively. **B.** At E6.5, *Cables2* was expressed ubiquitously in both extra- and embryonic parts in wild-type (left), in comparison with homozygous mutant (right). Antisense *Cables2* probe was used for WISH to confirm that *Cables2*-deficient embryos lacked expression. Scale bar, 100 µm.
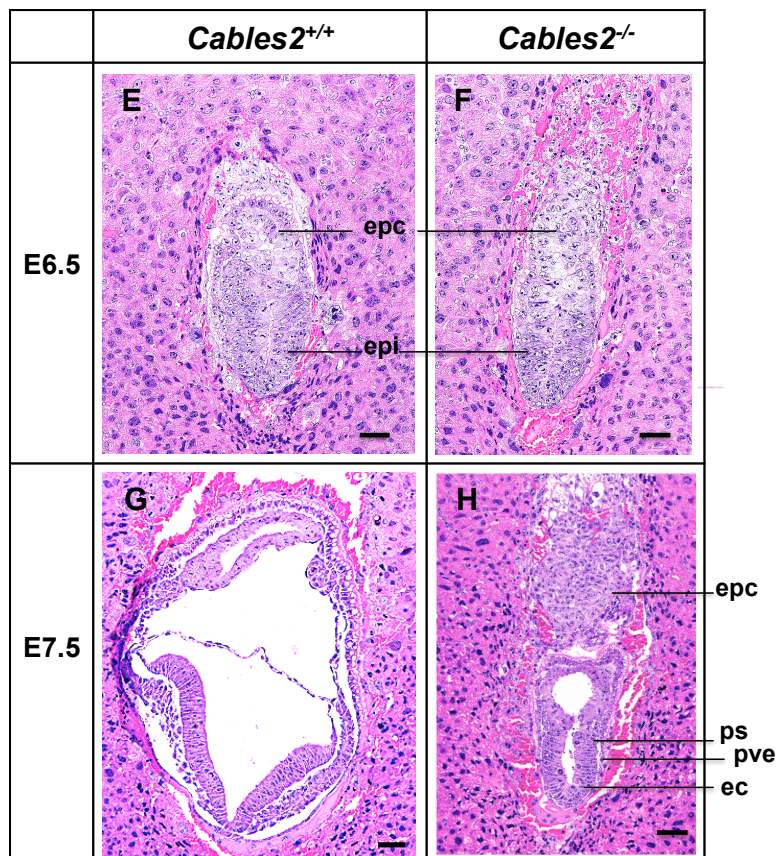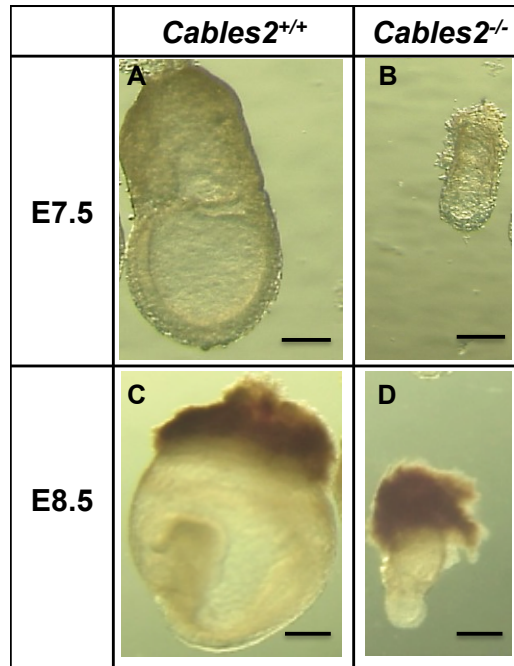
Figure 3. Morphological and histological analysis of *Cables2*-deficient embryos at early stages of development

Embryos were collected and genotyped at E7.5 **(A, B)** and E8.5 **(C, D)**. Histological analysis was on HE-stained sections. Wild-type and *Cables2* mutant embryos were embedded in paraffin and stained at E6.5 **(E, F)** and E7.5 **(G, H)**. epc: extra-placenta cone, ps: primitive streak; pve: posterior viscera endoderm; ec: ectoderm; epi: epiblast. Scale bars, 100 μm **(A-D)**, 50 μm **(E-H)**.
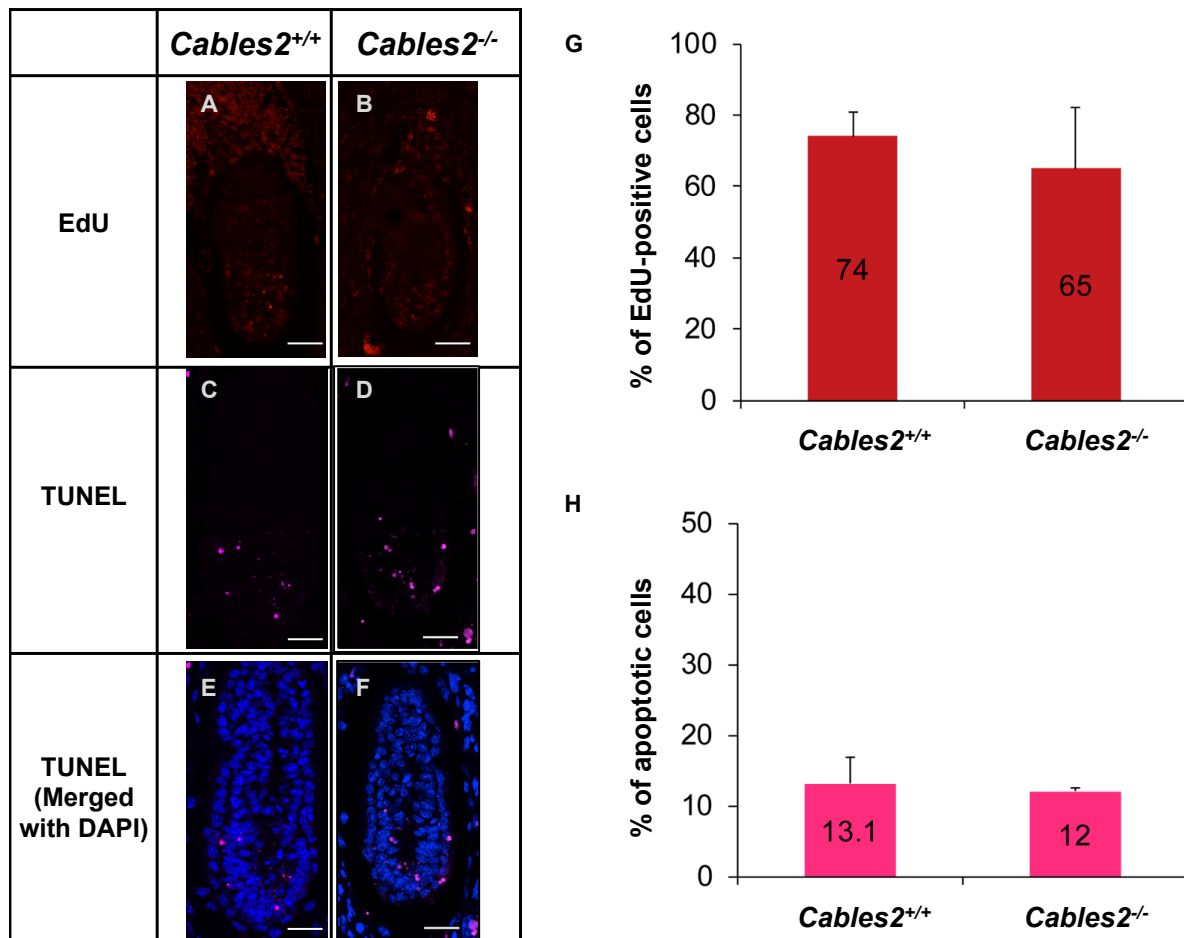
Figure 4. Proliferating and apoptotic cells in E6.5 *Cables2* mutant embryos

A-B. The EdU-incorporating cells represented the proliferation of cells in both wild-type and *Cables2*-deficient embryos (*n*=4). **C-F.** Apoptotic cells were detected in both wild-type and *Cables2*-deficient embryos (*n*=3). **G, H.** Compared with wild-type, *Cables2*-deficient embryos showed similar average percentages of cell proliferation and apoptotic cells. The average percentage was calculated by number of counted cells normalized to total number of cells within the embryo. At least 2 slides were counted per embryo. Y error bars: Standard of deviation (SD). Statistical significance was determined using Student's *t* test (*P* < 0.05). Scale bars, 50 μm.
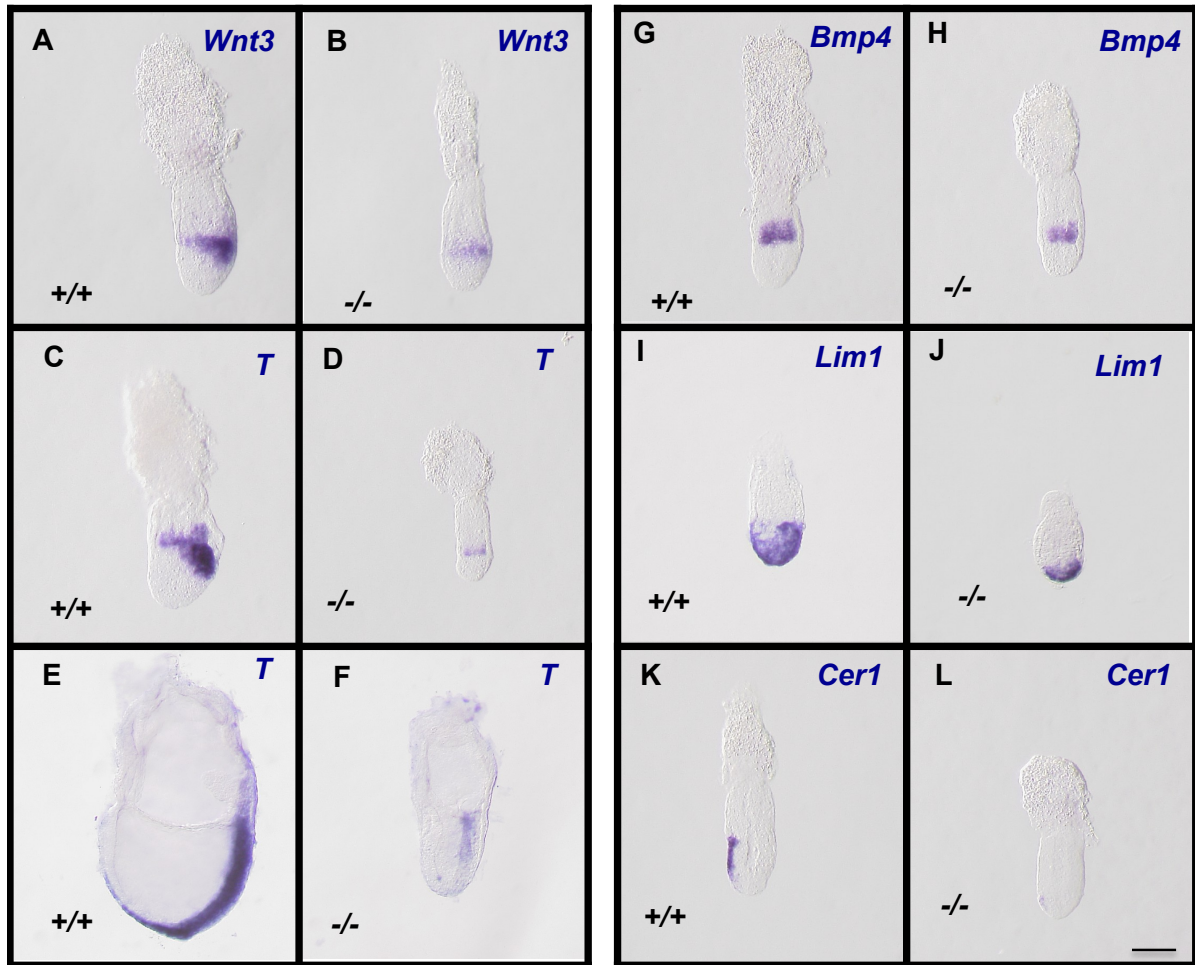
Figure 5. Expression of gastrulation markers in *Cables2*-deficient embryos

All embryos were collected, genotyped, and used for WISH at E6.5, except (E) and (F) were embryos at E7.5. Several key gastrulation markers were examined using both wild-type and *Cables2*-deficient embryos: *Wnt3* (*n*=5/3, respectively), *T* (*n*=7/5 at E6.5 and *n*=5/4 at E7.5), *BMP4* (*n*=4/3), *Lim1* (*n*=6/3), *Cer1* (*n*=3/3). Scale bar, 100 μm.
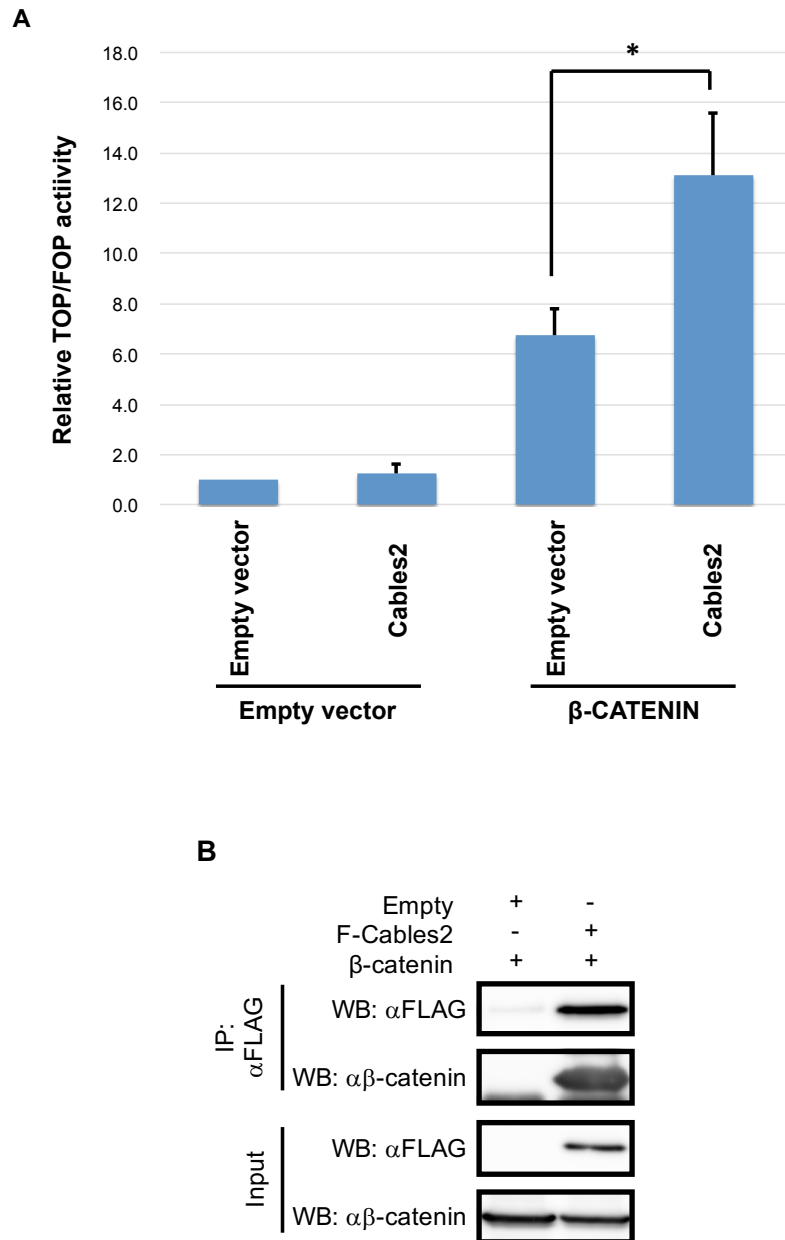
Figure 6. Enhancement of β-catenin activity by Cables2

A. 293FT cells were transfected with either TOPflash or FOPflash reporter vectors. Luciferase activity was measured after overnight culture. Results are expressed as relative TOP/FOP activity. Cables2 was associated with significantly increased TOP/FOP reporter activity. Columns: Averages of at least three independent experiments performed in triplicate. Y error bars: Standard deviation (SD). Statistical significance was determined using Student's t test ($P < 0.05$). **B.** Co-IP was performed

with FLAG-Cables2 and β-catenin expression vectors. The results obtained using anti-FLAG and anti-β-catenin antibodies showed the appearance of β-catenin in the precipitated complexes with Cables2.
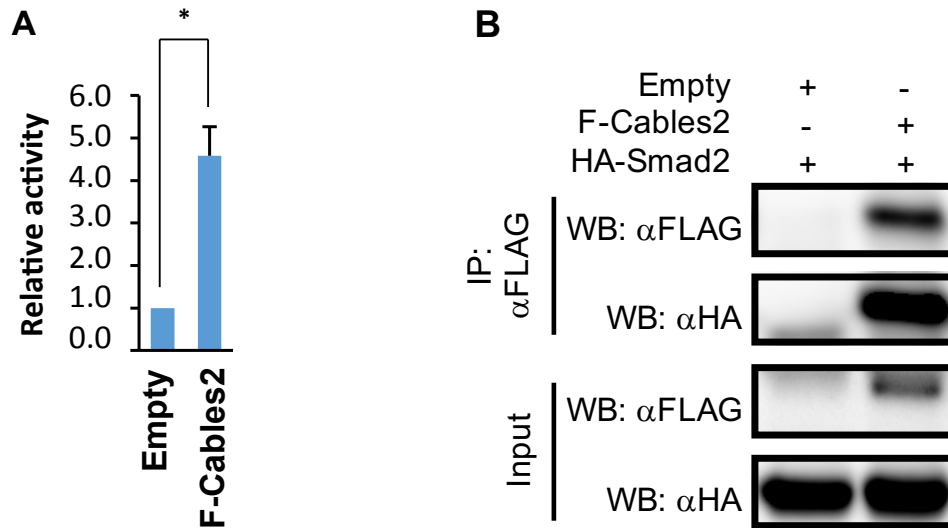
Figure 7. Activation of Smad2 by Cables2 *in vitro*

A. Cables2 and Smad2 interaction was examined using luciferase reporter vectors. Luciferase activity in 293FT cells was measured after overnight culture. Cables2 significantly increased ARE-luc reporter activity by about 4.5-fold compared to cells transfected with empty vector. Columns: Averages of at least three independent experiments performed in triplicate. Y error bars: Standard deviation (SD). Statistical significance was determined using Student's *t* test ($P < 0.05$). **B.** FLAG-Cables2 and HA-Smad2 expression vectors in Co-IP showed the physical interaction of Smad2 with Cables2.
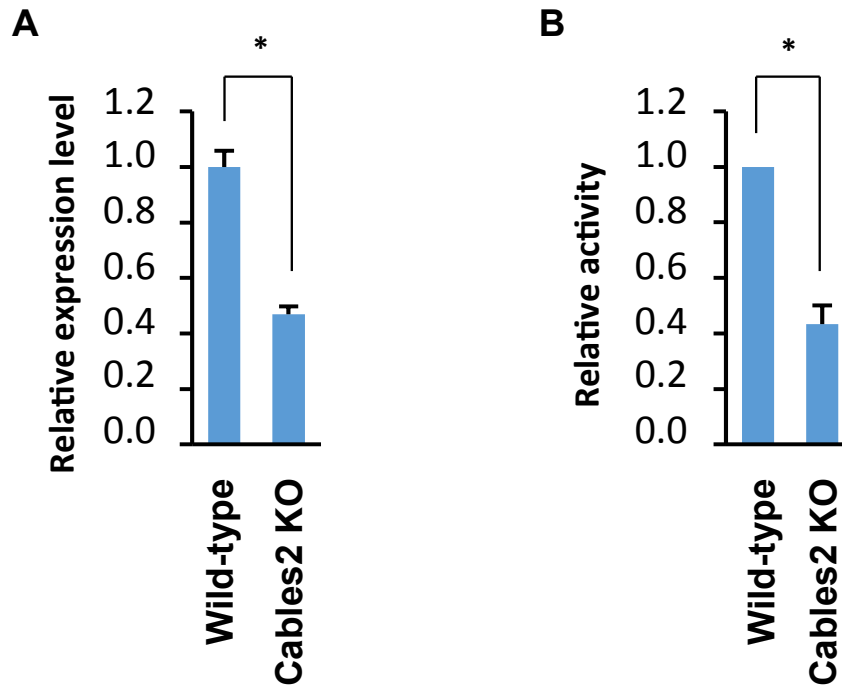
Figure 8. Downregulated *Nanog* expression and *Nanog* promoter activity in EpiLCs lacking *Cables2*

EpiLCs were induced from homozygous *Cables2* mutant ESCs. RT-qPCR **(A)** and *Nanog*-luc assay **(B)** consistently showed decreased expression of *Nanog* in *Cables2*-deficient cells compared with wild-type EpiLCs. Columns: Averages of at least three independent experiments performed in triplicate. Y error bars: Standard deviation (SD). Statistical significance was determined using Student's *t* test ($P <$ 0.05).
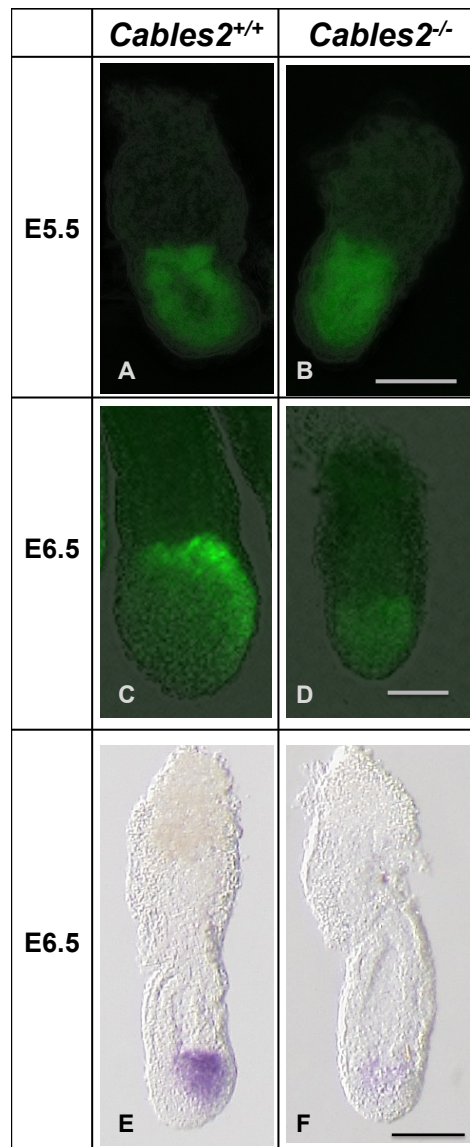
Figure 9. Nanog expression in *Cables2*-deficient embryos carrying *Nanog*-GFP

A-B. There was no difference between wild-type and mutant embryos at E5.5. **C-D.** All embryos in the same litter were collected at E6.5, and those with GFP-positive cells were compared. Cables2-deficient embryos showed faint and ectopic expression of the *Nanog*-GFP signal. **E-F.** *Nanog* expression in *Cables2* mutant was weaker and located even in the epiblast compare with wild-type (*n*=4). Scale bars, 50 μm **(A, B)**, 100 μm **(C-F)**.
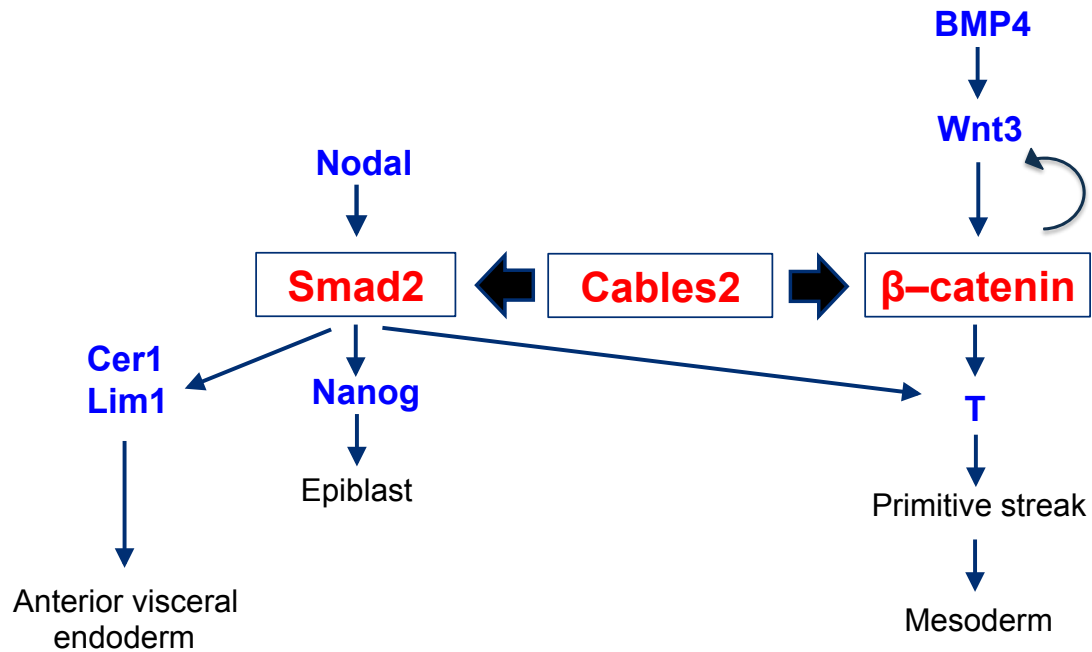
Figure 10. Proposed model for functional role of Cables2 in gastrulation via interaction with β-catenin and Smad2

The data show that Cables2 acts to stimulate the activities of β-catenin and Smad2 pathways. Therefore, deletion of *Cables2* results in downregulation of Wnt3/β-catenin and Nodal/Smad2 signalling in A-P axis formation, and thus the gastrulation does not process to form germ layers in mouse embryos.

REFERENCES

Truncated Cables1 causes agenesis of the corpus callosum in mice

Seiya Mizuno[1,6], Dinh TH Tra[1,6], Atsushi Mizobuchi[1], Hiroyoshi Iseki[1,2], Saori Mizuno-Iijima[1], Jun-Dal Kim[3], Junji Ishida[3], Yoichi Matsuda[4], Satoshi Kunita[5], Akiyoshi Fukamizu[3], Fumihiro Sugiyama[1] and Ken-ichi Yagami[1]

Agenesis of the corpus callosum (ACC) is a congenital abnormality of the brain structure. More than 60 genes are known to be involved in corpus callosum development. However, the molecular mechanisms underlying ACC are not fully understood. Previously, we produced a novel transgenic mouse strain, TAS, carrying genes of the tetracycline-inducible expression system that are not involved in brain development, and inherited ACC was observed in the brains of all homozygous TAS mice. Although ACC was probably induced by transgene insertion mutation, the causative gene and the molecular mechanism of its pathogenesis remain unclear. Here, we first performed interphase three-color fluorescence *in situ* hybridization (FISH) analysis to determine the genomic insertion site. Transgenes were inserted into chromosome 18 ∼12.0 Mb from the centromere. Gene expression analysis and genomic PCR walking showed that the genomic region containing exon 4 of *Cables1* was deleted by transgene insertion and the other exons of *Cables1* were intact. The mutant allele was designated as *Cables1^TAS*. Interestingly, *Cables1^TAS* mRNA consisted of exons 1–3 of *Cables1* and part of the transgene that encoded a novel truncated Cables1 protein. Homozygous TAS mice exhibited mRNA expression of *Cables1^TAS* in the fetal cerebrum, but not that of wild-type *Cables1*. To investigate whether a dominant negative effect of Cables1^TAS or complete loss of function of Cables1 gives rise to ACC, we produced *Cables1*-null mutant mice. ACC was not observed in *Cables1*-null mutant mice, suggesting that a dominant negative effect of Cables1^TAS impairs callosal formation. Moreover, ACC frequency in *Cables1^{+/TAS}* mice was significantly lower than that in *Cables1^{-/TAS}* mice, indicating that wild-type *Cables1* interfered with the dominant negative effect of *Cables1^TAS*. This study indicated that truncated Cables1 causes ACC and wild-type Cables1 contributes to callosal formation.

Laboratory Investigation advance online publication, 16 December 2013; doi:10.1038/labinvest.2013.146

KEYWORDS: ACC; Cables1-null mutant mice; TAS mouse; transgene insertion mutation; truncated Cables1

The corpus callosum is the largest fiber tract in the brain, consisting of 200–350 million and 7 million fibers in humans and mice, respectively,[1,2] and serves as a bridge to transfer information between the right and left cerebral hemispheres. Agenesis of the corpus callosum (ACC), which is characterized by absence of the corpus callosum,[3] is a congenital brain abnormality that may occur in isolation or in association with other central nervous system or systemic malformations in humans. Neonatal and prenatal imaging studies have suggested that ACC occurs in at least 1:4000 live births in the human population.[4,5] In other studies, the estimated incidence rates of ACC were reported as 3–5% of patients with neurodevelopmental disorders and 2–3% of the population with mental impairment.[6–8]

Reverse genetic analyses of mice identified more than 60 causative genes of ACC, and these genes are involved in several processes in the formation of corpus callous.[9] The *Sp8*, *Pax6*, and *Otx2* genes are essential for patterning of the developing forebrain. Analyses of mouse strains with mutations in these genes indicated their involvement in ACC with multiple brain malformations and strong craniofacial abnormalities.[10–12] As both brain midline fusion defects and ACC were observed in several inbred mouse strains (eg, BALBc/Wah1 and 129/J),[13] telencephalic

[1]Laboratory Animal Resource Center, University of Tsukuba, Tsukuba, Japan; [2]Project Research Division, Research Center for Genomic Medicine, Saitama Medical University, Saitama, Japan; [3]Life Science Center, Tsukuba Advanced Research Alliance, Graduate School of Life and Environmental Sciences, University of Tsukuba, Tsukuba, Japan; [4]Laboratory of Animal Genetics, Graduate School of Bioagricultural Sciences, Nagoya University, Nagoya, Japan and [5]Center for Experimental Medicine, Jichi Medical University, Shimotsuke, Japan
Correspondence: Dr F Sugiyama, PhD, Laboratory Animal Resource Center, University of Tsukuba, 1-1-1 Tennodai, Tsukuba 305-8575, Japan.
E-mail: bunbun@md.tsukuba.ac.jp
[6]These authors contributed equally to this work.
Received 27 August 2013; revised 7 November 2013; accepted 8 November 2013; published online 16 December 2013

midline fusion appears to be necessary for corpus callosum development. Correct development of the cerebral cortex is also important for formation of the corpus callosum because callosal neurons, which extend axons across the corpus callosum, are located in the cerebral cortex. Indeed, *N-cadherin* gene-mutant mice showed ACC because of abnormal development of the cerebral cortex.[14] Furthermore, the projection of callosal axons from the cortex is regulated by various axon guidance molecules, including Slit/Robo, Netrin/DCC, Ephs/Ephrins, and Semaphorins/Neuropilins. Indeed, abnormal corpus callosum development has been reported in mice with deficiencies in these genes.[15–22]

Occasionally, random integration of transgene DNA into the host genome disrupts an endogenous gene and causes a class of mutations called transgene insertion mutations.[23] Approximately 5–15% of random DNA insertion events in transgenic mice are associated with an abnormal phenotype by transgene insertion mutation.[24] The integrated transgene may affect endogenous loci close to the transgene and result in inactivation of the endogenous gene or creation of a fusion with an endogenous gene. When transgene insertion mutation results in unexpected phenotypic alterations in mice, knowledge regarding the precise location of transgene insertion within the genome could be useful to discover genes responsible for defects.

Previously, we developed a transgenic mouse strain, TAS (reverse *t*etracycline-controlled trans*a*ctivator and tetra-cycline-controlled transcriptional *s*ilencer), that showed ACC accompanied with formation of Probst bundles, as seen in human patients.[25] The complete penetrance of ACC was observed in homozygous TAS mice. Furthermore, axons of the corpus callosum were not repelled by the midline structures. TAS mice carry both the reverse tetracycline-controlled transactivator (rtTA) gene and the tetracycline-controlled transcriptional silencer gene (tTS) in the BALB/c genetic background. As these transgene products do not affect brain development and another founder line carrying both rtTA and tTS did not exhibit ACC, we hypothesized that ACC in TAS was caused by transgene insertion mutation. In addition, we reported previously that rtTA and tTS were located in the region between 9.3 and 16.9 Mb from the centromere on chromosome 18 in TAS, and there is no critical gene known to be involved in ACC in the candidate genomic region.

Although ACC in TAS mice is probably induced by transgene insertion mutation, the causative gene and its pathological mechanism have not yet been clarified. Here, we identified the genomic insertion site of the transgene on chromosome 18 at ∼12 Mb from the centromere by multicolor fluorescence *in situ* hybridization (FISH) analysis. Furthermore, the insertional mutation was shown to generate a novel mutant *Cables1* allele. Analysis of *Cables1*-null mutant mice indicated that complete loss of function of Cables1 did not contribute to callosal malformation. Finally, we demonstrated that the frequency of ACC in *Cables1*$^{+/TAS}$

mice was significantly lower than that in *Cables1*$^{-/TAS}$ mice. These data suggest that ACC in TAS mice is caused by the N-terminal half of Cables1, a molecule responsible for the complex organization of the corpus callosum.

MATERIALS AND METHODS
Animals
The TAS mice used in this study have been described previously.[25] BALB/cAJ, C57BL/6J, and ICR mice were purchased from CLEA Japan. Animals were kept as described previously.[25] Animal experiments were carried out humanely in accordance with the Regulations for Animal Experiments of the University of Tsukuba and Fundamental Guidelines for Proper Conduct of Animal Experiment and Related Activities in Academic Research Institutions under the jurisdiction of the Ministry of Education, Culture, Sports, Science, and Technology of Japan and with approval from the Institutional Animal Experiment Committee of our university.

KB Staining
The brains of adult mice were rapidly immersed in 10% neutral buffered formalin for at least 1 week before embedding. Subsequently, brains were dehydrated by passage through an ascending series of alcohol concentrations, cleared in xylene, and embedded in paraffin. Paraffin blocks were cut into serial sections 6 μm thick on a microtome and mounted on glass slides. Sections were stained with Klüver–Barrera (KB) stain according to standard protocols.

Immunofluorescence
The neonatal brains were fixed in 4% paraformaldehyde in PBS. After overnight fixation at 4 °C, the brains were cryo-protected in 30% sucrose and frozen in OCT compound (Sakura Finetek). Cryostat sections 30 μm thick were blocked with 0.2% Triton X-100 in SuperBlock® Blocking Buffer in TBS (Pierce). The sections were incubated with rat anti-L1CAM antibody (1:100; Millipore). Subsequently, the sections were washed in PBS and incubated with mouse Cy3-GFAP antibody (1:200; Sigma) and Alexa Fluor 350 goat anti-rat IgG (1:200; Life Technologies).

FISH
R-banded chromosome preparations were made from the spleen lymphocytes of heterozygous TAS mice as previously described.[25] After hardening at 65 °C, the chromosome spreads were denatured in 70% formamide/2× SSC for 2 min, then dehydrated in ethanol (70 and 100%) at 4 °C for 15 min. RP23-232N9 and RP23-101N14 bacterial artificial chromosome (BAC) DNAs were purified by NucleoBond BAC 100 (Macherey-Nagel). These BAC and tTS DNA probes were labeled by nick translation (Roche) with biotin-dUTP (Roche), Cy3-dUTP (GE Healthcare), and Cy-5-dUTP (GE Healthcare), respectively. Repeat sequences in BAC DNA probes were blocked with 10 μg Cot1 DNA (Life Technologies). Aliquots of 1 μg of each BAC probe and

500 ng of tTS DNA probe in formamide were denatured at 75 °C for 10 min and applied to slides with hybridization buffer containing 200 μg/μl dextran sulfate sodium salt (Sigma), 200 μg/μl bovine serum albumin (Roche), and 2 × SSC. After overnight hybridization at 37 °C, the slides were washed in 1 ×, 2 ×, and 4 × SSC and incubated with avidin-FITC (Roche) at 37 °C for 1 h.

RT-PCR
Total RNA was prepared from the brains of embryos using ISOGEN (Nippon Gene). cDNA was synthesized as described previously.[25] PCR was performed with AmpliTaq Gold® PCR Master Mix (Life Technologies) and various primers (Supplementary Table 1).

Sequencing
Genomic and cDNA sequencing analyses were performed with a BigDye® Terminator v3.1 Cycle Sequencing Kit and Applied Biosystems 3130 Genetic Analyzer (Life Technologies).

Northern Blotting
Aliquots of 10 μg of total mouse embryonic cerebral RNA (E17.5 and E19.5) were denatured, fractionated, and transferred onto Hybond N$^+$ (GE Healthcare) according to standard protocols. The 5′- and 3′-cDNA probes were derived from mouse brain cDNA with specific primers (Supplementary Table 2). Hybridization and detection were performed using a DIG Northern Starter Kit (Roche).

Transfection and Western Blotting
cDNA fragments of *Cables1* and *Cables1*^{TAS} CDS, which were derived from wild-type and TAS mice, were introduced into the pc3 mammalian expression vector. These constructs were transfected into HEK293T cells by LipofectAMINE LTX (Life Technologies). Cables1 and Cables1^{TAS} proteins from transfected cells were detected with rabbit anti-N-terminal Cables1 antibody (M280; 1:100; Santa Cruz) and HRP-conjugated donkey anti-rabbit IgG secondary antibody (1:4000; GE Healthcare).

Gene Targeting
The *Cables1*^{null} targeting vector contained the *Neo*^{r} cassette (Figure 5a). The 3.8-kb 5′-homology arm and 4.6-kb 3′-homology arm were amplified from BALB/c mouse genomic DNA with Cables1^{null} specific primers (Supplementary Table 3). The *Cables1*^{null} targeting vector was introduced into BALB/c embryonic stem cells by electroporation.[26] Genomic DNA from G418-resistant colonies were screened for homologous recombination by Southern blotting.

RESULTS
Identification of Transgene Insertion Site in TAS Mice
We recently developed a novel transgenic mouse strain carrying rtTA and tTS, the components of the Tet-on/off gene expression system. Unexpectedly, only one line of transgenic mice showed ACC (Figure 1b), designated as TAS.[25] As rtTA and tTS have not been reported to affect cerebral development, we hypothesized that ACC in TAS mice was due to disruption of an endogenous gene by transgene insertion. A recent study showed that both rtTA and tTS transgenes are closely linked and inserted into the region between 9.3 and 16.9 Mb from the centromere on chromosome 18 in TAS mice.

To narrow down the insertion site, we performed three-color FISH analyses. The DNA probes from BAC clones RP23-232N9 (derived from chr.18: 11 108 363 to 11 290 545) and RP23-101N14 (derived from chr.18: 12 743 636 to 12 933 531) were labeled with Cy3 and Cy5, respectively. A transgenic DNA probe was labeled with FITC. Although these three-color signals were detected on chromosome 18, the signals were not separated on metaphase chromosome spreads (Figure 2a). In contrast, the FITC signal was detected between Cy3 and Cy5 signals on interphase chromosome spreads (Figure 2b). These observations indicated transgene insertion in the region between 11.3 and 12.7 Mb on chromosome 18 (Figure 2c). We then examined the expression of 14 genes located around the region of transgene insertion (Figure 2c). RT-PCR analyses indicated that only the *Cables1* gene expression pattern was different between TAS and wild-type mice (Figure 2d).

Exon 4 of *Cables1* Is Disrupted by Transgene Insertion
The *Cables1* gene is located 12 Mb from the centromere on mouse chromosome 18. *Cables1* consists of 10 exons, and alternative splicing results in two transcripts. Exon 4 of *Cables1* isoform I is not included in isoform II (Figure 4c). We performed genomic PCR walking in the *Cables1* locus to determine the transgene insertion site. Consistent with the results of RT-PCR analyses, long-PCR (data not shown) and sequence analyses (Figure 3a) showed that the genomic region from 12 058 849 to 12 070 825 bp on chromosome 18, including exon 4 of *Cables1*, was deleted by transgenes insertion (Figure 3b). The novel mutant allele of *Cables1* was designated as *Cables1*^{TAS}. As multiple copies of the transgenes (rtTA and tTS) were inserted into the genome,[25] no amplification product was obtained from *Cables1*^{TAS} by genomic PCR analysis with a primer set derived from the 5′ and 3′ flanking regions of the deletion (data not shown).

De Novo Truncating Mutation in *Cables1*
No amplification of *Cables1* cDNA was observed in TAS homozygous mutant mice by RT-PCR analysis using primers derived from exons 2 and 7 (Figure 2d). In addition, genomic analysis revealed that only exon 4 of *Cables1* was deleted (Figure 3b). These results suggested that truncated *Cables1* mRNA, including exons 1–3, may be expressed in TAS mice. Next, we investigated *Cables1* expression in the fetal cerebrum at E17.5 and 19.5, because the corpus callosum dramatically develops late in gestation. Northern blotting
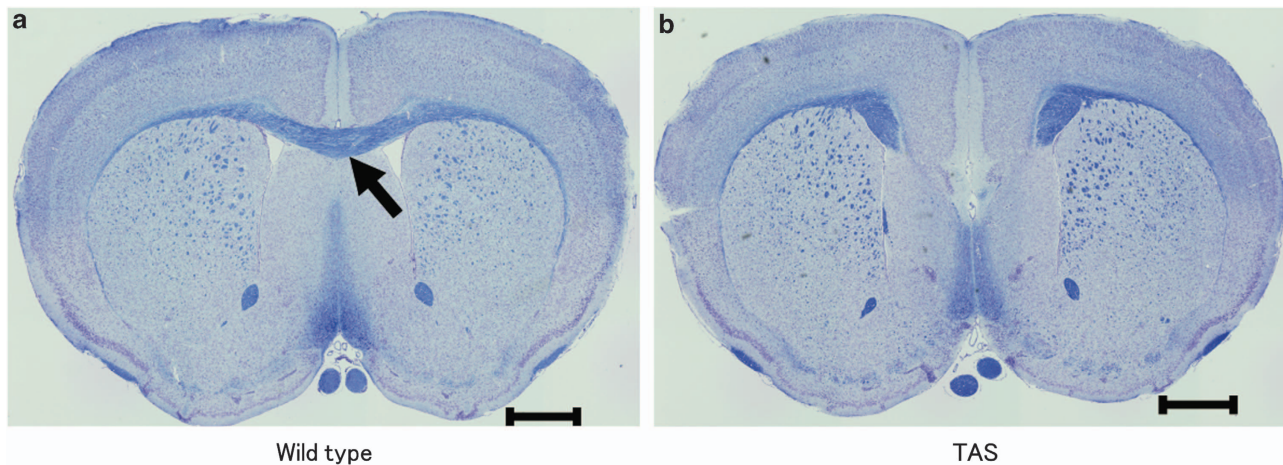
Figure 1 Agenesis of the corpus callosum in TAS. Coronal sections through the rostral levels of the cerebrum in adult wild-type (**a**) and adult TAS (**b**) mice were stained with Klüver–Barrera (KB). Arrow indicates the corpus callosum; scale bar = 1 mm (**a**, **b**).

analysis with 5'-cDNA probe (derived from part of exons 1–3) revealed that *Cables1* mRNA was shorter in TAS fetuses (*Cables1$^{TAS/TAS}$*) than in wild-type fetuses. In contrast, no band was detected in TAS fetuses (*Cables1$^{TAS/TAS}$*) with 3'-cDNA probe derived from exons 7–9 (Figure 4a). These results suggested that exons 1–3 of *Cables1* are included in *Cables1^{TAS}* mRNA and the other exons are not transcribed in TAS (*Cables1$^{TAS/TAS}$*). In addition, *Cables1^{TAS}* mRNA more than 2 kb in length was detected with 5'-cDNA probe, even though a 1425-bp fragment comprising exons 1–3 of *Cables1*. Sequence analysis was then performed to investigate *Cables1^{TAS}* mRNA in detail. Interestingly, exons 1–3 of *Cables1* mRNA were linked to the transgene in *Cables1^{TAS}* (Figure 4b). Furthermore, a frameshift mutation was detected in the transgene following exon 3 of the *Cables1^{TAS}* transcript, resulting in a stop codon (TAG) 69 bp downstream from the exon 1–3 boundary (Figure 4c).

To confirm whether a mutant small protein is translated from *Cables1^{TAS}*, HEK293T cells were transfected with *Cables1^{TAS}* or wild-type *Cables1* expression vector. As expected, western blotting analysis with an antibody to the N-terminus of Cables1 (M-280) indicated that mutant protein derived from *Cables1^{TAS}* was smaller than the wild-type protein (Figure 4d). Furthermore, the molecular weight of the mutant protein product from *Cables1^{TAS}* was similar to the predicted size (33.5 kDa). These results suggested that the abnormal truncated (N-terminal half) Cables1 protein could be expressed in TAS mice. Western blotting analysis was then performed to detect truncated Cables1 in the brain of these mice. However, anti-Cables1 antibody (M-280) did not specifically detect wild-type or truncated Cables1 protein in brain lysate (data not shown).

Development of Normal Corpus Callosum in *Cables1*-Null Mutant Mice
Although reverse genetics analyses indicated various abnormalities in *Cables1*-deficient mice (eg, development of

endometrial hyperplasia, progression of colon cancer, and poor oocyte quality),[27–29] the effect of *Cables1*-null mutation on the corpus callosum has not been reported. To determine whether null or TAS mutation gives rise to ACC, it is necessary to establish Cables1-deficient mice in the BALB/c genetic background, because ACC in TAS was seen with the BALB/c (not C57BL/6) genetic background.[25] We successfully produced *Cables1*-null mutant mice in the BALB/c genetic background (Figures 5a–c). The targeting vector was introduced into BALB/c embryonic stem cells by electroporation.[26] Five distinct clones were obtained, one of which (clone 10) was used to generate germline chimeras by aggregation with tetraploid ICR mouse embryos. *Cables1$^{-/-}$* mice were obtained from intercrosses of *Cables1$^{-/+}$* mice at Mendelian ratios. These mice were genotyped by genomic Southern blotting (Figure 5b), and RT-PCR analysis with primers derived from exons 2 and 7 revealed that *Cables1* was not expressed in *Cables1$^{-/-}$* mice (Figure 5c). We then confirmed that a normal corpus callosum was formed in the brains of all *Cables1$^{-/-}$* adult mice examined (n = 7; Figure 5d). These data indicated that lack of *Cables1* function is not responsible for ACC in TAS mice.

Relationship between *Cables1* Genotype and ACC
To understand the relationship between the *Cables1* genotype and ACC phenotype in more detail, *Cables1$^{+/TAS}$* mice were crossed with *Cables1$^{-/-}$* mice. As a result, we obtained eight *Cables1$^{+/TAS}$* and 6 *Cables1$^{-/TAS}$* mice and examined gross callosum structures at 0 days of age by immunofluorescence with L1-CAM and GFAP antibodies. Similar to *Cables1$^{TAS/TAS}$*, all of the *Cables1$^{-/TAS}$* mice showed ACC (Figure 6b). In our previous study, all *Cables1$^{TAS/TAS}$* (n = 12) and 62% of *Cables1$^{+/TAS}$*(n = 37) mice developed ACC.[25] The *Cables1* genotypes and frequency of ACC are summarized in Table 1. Taken together, these results indicated that ACC occurred only in mice bearing the *Cables1^{TAS}* allele. These data indicated that ACC is caused not
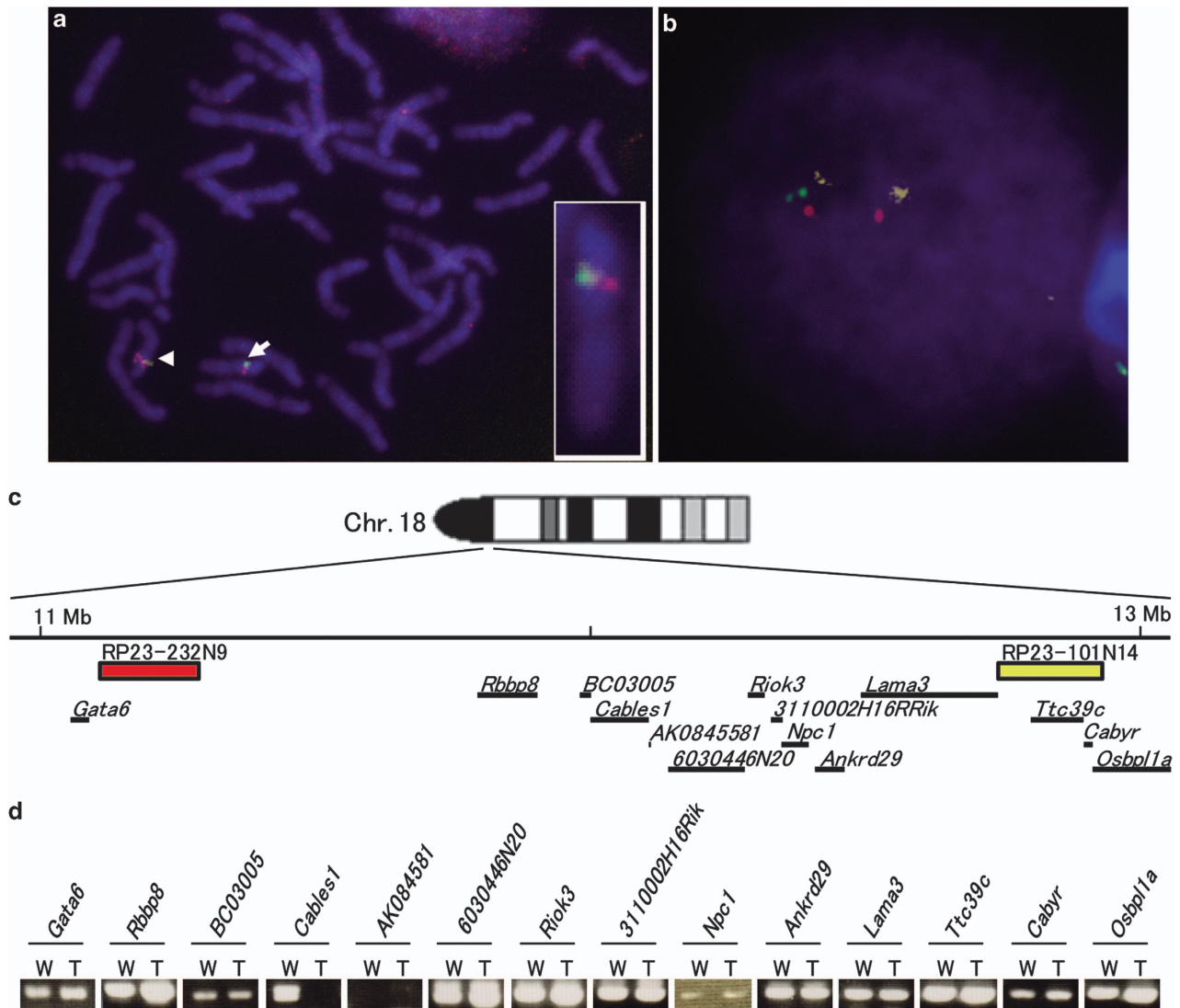
Figure 2 Identification of transgene insertion site. (**a**) FISH to metaphase heterozygous TAS chromosome spreads. The arrow indicates transgene (green) signals colocalized with RP23-232N9 (red) and RP23-101N14 (yellow). The white box shows an enlarged view of this chromosome and indicates that the three-color signals are not separated. The arrowhead indicates red and yellow signals on the nontransgenic chromosome. (**b**) FISH to interphase heterozygous TAS chromosome spreads. Transgene (green) signals were observed between RP23-232N9 (red) and RP23-101N14 (yellow) signals. (**c**) The genomic region between RP23-232N9 (red box) and RP32-101N14 (yellow box) contains 14 known and predicted genes. (**d**) RT-PCR analysis of the 14 genes showed that only the *Cables1* gene expression pattern was different between TAS and wild-type mice. W, wild-type mouse; T, TAS mouse.

by loss of *Cables1* function but by *Cables1*[TAS] mutation. Interestingly, as ACC frequency in *Cables1*[+/TAS] mice was lower than that in *Cables1*[−/TAS] mice, wild-type *Cables1* interfered with the dominant negative effect of *Cables1*[TAS], suggesting that wild-type Cables1 may be involved in corpus callosum development.

DISCUSSION

TAS mice are a useful model in which to investigate genes involved in regulation of corpus callosum development and to gain new insights into the molecular genetics of ACC.[25] Here we showed that exon 4 of *Cables1* was deleted by transgene insertion mutation in TAS mice. We also showed that the

abnormal *Cables1* mRNA, which is composed of exons 1–3 of *Cables1* and a short part of the transgene, was expressed in the TAS mouse fetal brain. In addition, truncated Cables1 protein was shown to be generated from *Cables*[TAS] transcript. The callosal appearance in *Cables1*-null mutant mice supported the conclusion that ACC in TAS mice is because of the dominant negative effect of *Cables*[TAS] mutation on callosal organization. Moreover, we showed the relationship between *Cables1* genotype and ACC, demonstrating the contribution of wild-type Cables1 to callosal formation.

Three-color interphase FISH analyses revealed transgene insertion in the region between 11.3 and 12.7 Mb from the centromere of chromosome 18 in TAC mice (Figures 2b
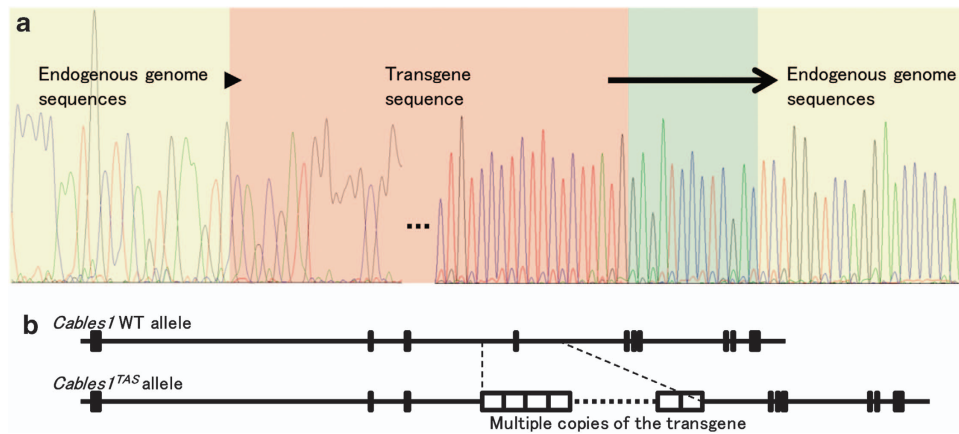
Figure 3 Disruption of *Cables1* gene caused by transgene insertion. (**a**) Results of genomic sequencing analysis. The transgenic sequence (red background) was directly connected (arrowhead) to 5585 bp upstream of exon 4 of *Cables1* (yellow background). The 3′-end of the transgene connected (arrow) to neither the genomic nor transgenic sequence (green background) and subsequently connected to 6314 bp downstream of exon 4 (red background). Dotted line indicates multiple copies of the transgene. (**b**) The schematic diagram shows a comparison of *Cables1* genomic structure between wild-type and *TAS* alleles.
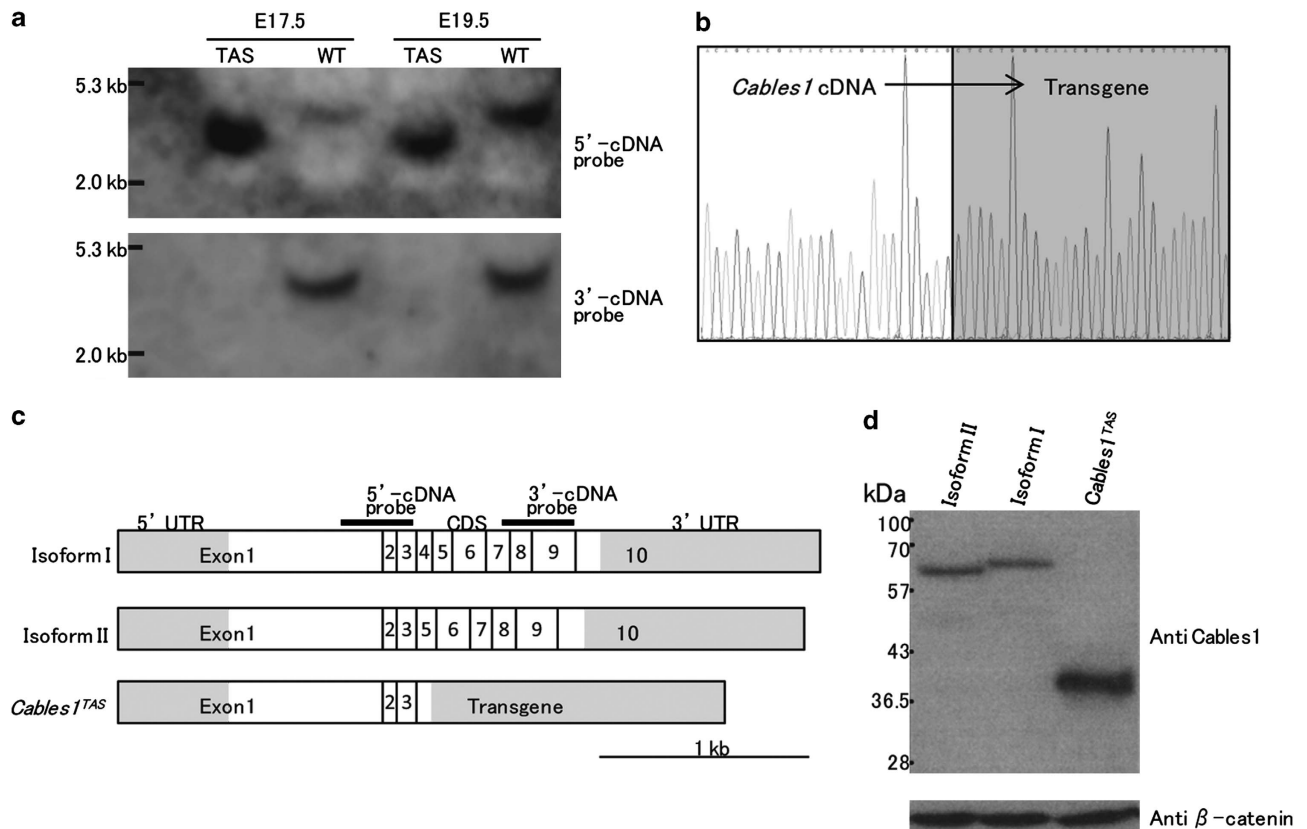
Figure 4 Mutated *Cables1* mRNA in TAS. (**a**) Northern blot analysis of *Cables1* in the fetal cerebrum of wild-type and TAS mice. Shorter mRNA derived from TAS was detected only with the 5′-cDNA probe. (**b**) cDNA sequencing analysis. The transgenic sequence (gray background) was directly connected (arrow) to the 3′-end of exon 3 (white background). (**c**) Three schematic diagrams indicating isoform I, isoform II, and TAS mutant *Cables1* mRNA. Gray and white boxes indicate untranslated region and coding sequence, respectively. (**d**) Three variants of Cables1 protein were expressed in HEK293T cells. These proteins were analyzed by western blotting. Cables1[TAS] protein was smaller than the wild type. UTR, untranslated region; CDS, coding sequence.

and c). A search in the UCSC genomic database (http://genome.ucsc.edu/) indicated that there are 14 genes in this genomic region. Figure 2d shows that there were no tran-

scriptional differences between wild-type and homozygous TAS mice for any of these genes except *Cables1*. Furthermore, we confirmed that there were no differences in the

Figure 5 Cables1-null mutant mouse. (**a**) Schematic of the null allele in which exon 1 was deleted by homologous recombination in BALB/c ES cells. X, Xb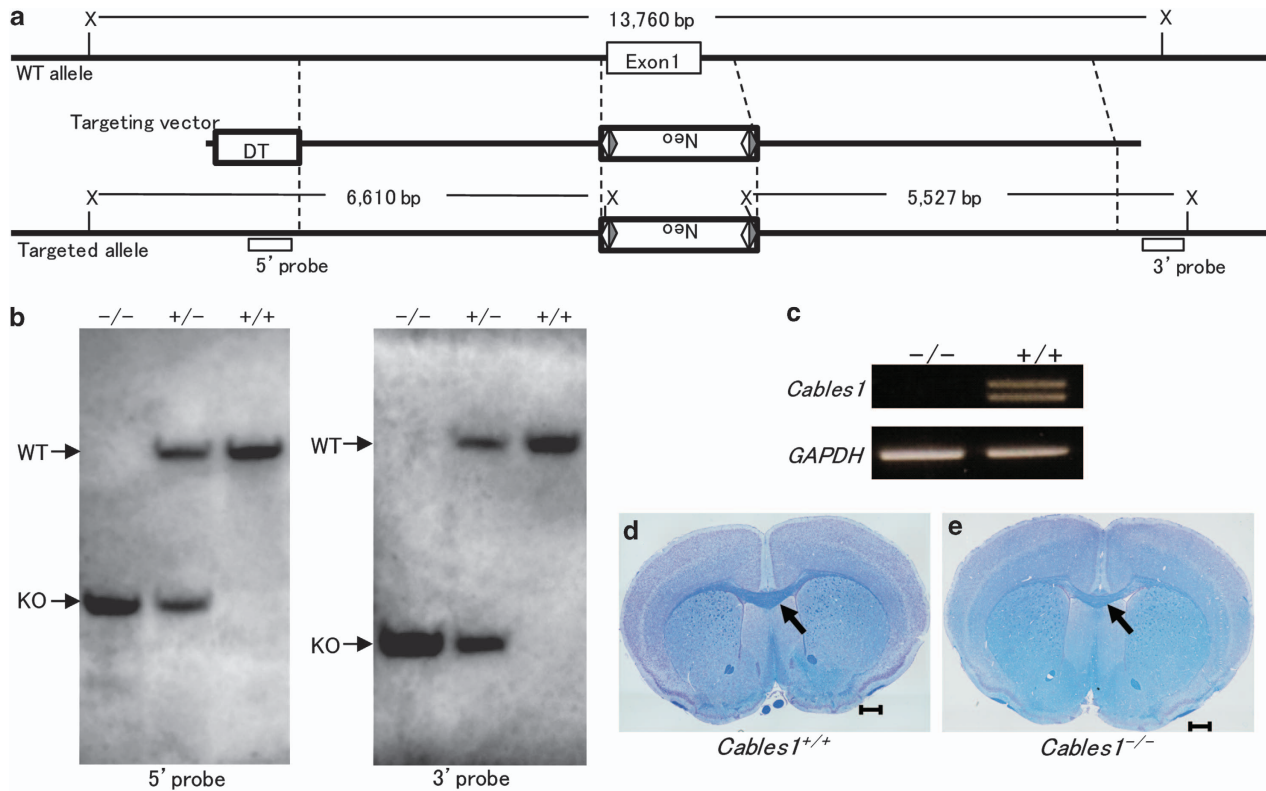aI site; Neo, neomycin resistance cassette; DT, diphtheria toxin cassette; white triangle, LoxP; gray triangle, FRT. (**b**) Southern blotting of genomic DNA derived from Cables1$^{+/+}$, Cables1$^{-/+}$, and Cables1$^{-/-}$ mice. (**c**) RT-PCR of Cables1 from exon 2 through exon 7 demonstrated the absence of both isoform I and isoform II Cables1 products in Cables1$^{-/-}$ mice. Coronal sections through the rostral levels of the cerebrum in adult Cables1$^{+/+}$ (**d**) and Cables1$^{-/-}$ (**e**) mice were stained with Klüver–Barrera (KB). Arrows indicate the corpus callosum; scale bar = 1 mm.
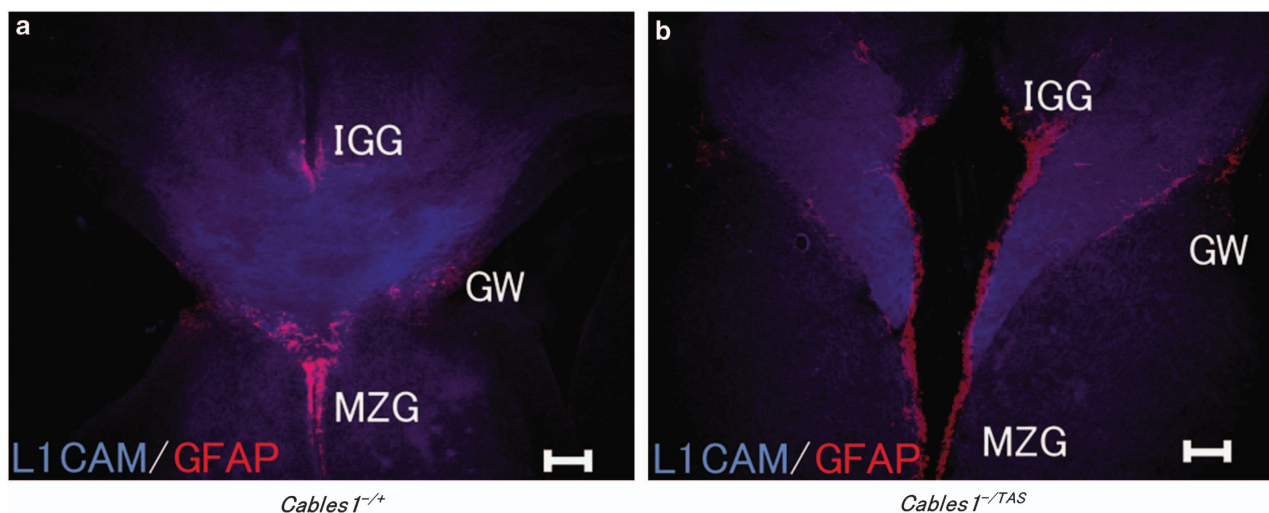
Figure 6 ACC in Cables1$^{-/TAS}$. Coronal sections in P0 Cables1$^{-/+}$ (**a**) and Cables1$^{-/TAS}$ (**b**). Staining with antibodies against L1CAM (blue) and GFAP (red). Callosal axons did not cross the midline, and GFAP-expressing IGG and MZG were indistinguishable from Cables1$^{-/TAS}$ (**b**). GW, glial wedge; IGG, indusium griseum glia; MZG, midline zipper glia; scale bar = 100 μm.

expression of 32 additional genes located in the vicinity of the candidate region between wild-type mice and homozygous TAS mice (data not shown). These results indicate that only Cables1 is disrupted by transgene insertion,

suggesting that ACC is caused by Cables1 gene mutation in TAS mice.

A complete CABLES1 is also present in the human genome and is mapped to the long arm of chromosome 18 at

20.71–20.84 Mb from the centromere (http://genome.ucsc.edu). *CABLES1*, originally called *iK3-1*, has been isolated using the yeast two-hybrid system with cyclin-dependent kinase 3 (CDK3) cDNA as bait to evaluate cdk3 function.[30] In addition to the interaction with CDK3, CABLES1 is functionally connected to p53 and p73 in cell death, suggesting that it is a molecule involved in harmonizing cell cycle progression and cell death.[31] Previous studies showed that *Cables1*-null mutant mice displayed increased cellular proliferation (eg, endometrial hyperplasia, colon cancer, and oocyte development).[27–29] In contrast to *Cables1* loss-of-function mutation, overexpression of *Cables1* in a colon cancer cell line showed tumor suppressor activity, including inhibition of colony formation and cell growth.[32] However, there have been no reports that aberrant expression of *Cable1* is involved in neural defects *in vivo*.

Zukerberg et al[33] showed that Cables1 is expressed in the brain, where it is present in postmitotic neurons of the cerebral cortex, and interacts directly with Cdk5 and Abl1 (Abelson murine leukemia viral oncogene homolog 1) in the brain lysate. Furthermore, Cables1 and Cdk5 were localized

at the tips of growing axons. They suggested that the association of Cables1 and Cdk5 is part of the signaling pathway that operates during brain development. Moreover, Rhee et al[34] demonstrated that Cables1 is the essential molecule connecting Robo-associated Abl and N-cadherin-associated β-catenin. Slit/Robo signaling is known to play a crucial role in cortical axon guidance across the corpus callosum by the midline glial population.[35] This is the first report regarding a *Cables1* allele associated with an acallosal phenotype. We also clearly showed that a novel *Cables1* mutation in TAS mice generates a truncated Cables1 product. These observations strongly suggest that Cables1 may be involved in development of the carpus callosum.

We produced a unique *Cables1*-null mutant strain derived from BALB/c ES cells to evaluate Cables1 function in BALB/c mice, because it is known that the genetic background has a strong influence on the development of ACC in mice.[12] Unexpectedly, the complete loss-of-function Cables1 mutant showed no alterations in callosal formation in mice, even with the same genetic background as TAS mice. Although we cannot as yet provide direct evidence for the lack of phenotype in the loss-of-function Cables1 mutant, the discrepancy in ACC frequency between $Cables^{+/TAS}$ mice (62%) and $Cables1^{-/TAS}$ mice (100%) is suggestive of the possible mechanism. In mice, expression of truncated Cables1 resulted in acallosal brain development and $Cables1^{TAS}$ gene dosage was associated with the incidence of ACC, indicating a dominant negative function of $Cables^{TAS}$ on callosal formation. In contrast, the absence of Cables1 had no negative influence on brain development, suggesting the presence of a molecule(s) functionally redundant to Cables1. Furthermore, the significantly lower frequency of ACC in $Cables1^{+/TAS}$ mice compared with $Cables1^{-/TAS}$ mice indicated that the wild-type Cables1 serves to form the corpus callosum. Therefore, one copy of $Cable1^{TAS}$ may be sufficient to impair the function of the homozygous redundant gene. This speculation is summarized in Figure 7.

Table 1 Frequency of ACC in *Cables1*-mutant mice

Genotype	No. of mice examined	No. of mice with ACC (%)[a]
Cables1$^{+/+}$	59	0 (0%)[b]
Cables1$^{+/TAS}$	37	23 (62%)[b]
Cables1$^{TAS/TAS}$	12	12 (100%)[b]
Cables1$^{-/-}$	7	0 (0%)
Cables1$^{-/TAS}$	6	6 (100%)

[a]No. of mice with ACC/no. of mice examined.
[b]These data were reported in our previous study.[25]
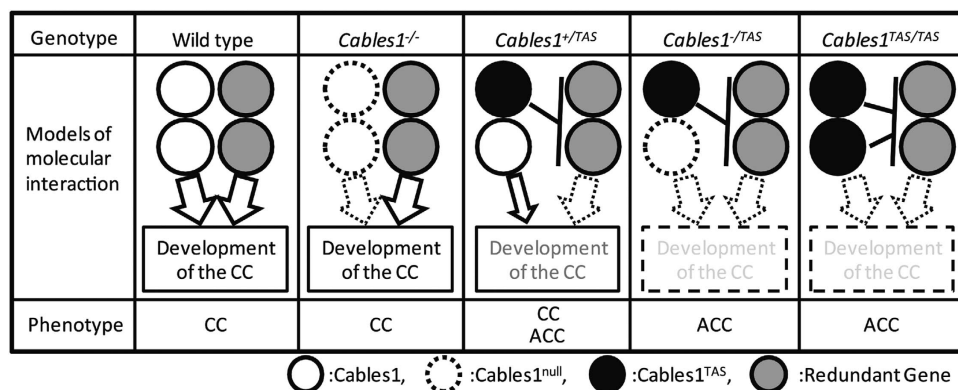
Figure 7 Model for gene interaction between *Cables1*, *Cables1*^{TAS}, and redundant gene. *Cables1* and its redundant gene play a role in the development of corpus callosum, and *Cables1*^{TAS} may impair redundant gene function. As the redundant gene functions in development of the corpus callosum, ACC was not observed in *Cables1*-null mutant mice. In heterozygous TAS mice (*Cables1*$^{+/TAS}$), even though redundant gene function was impaired by *Cables1*^{TAS}, one copy of the *Cables1* gene served to form the corpus callosum. In contrast, all *Cables1*$^{TAS/TAS}$ and *Cables1*$^{-/TAS}$ mice showed ACC because *Cables1* and its redundant gene were not expressed or were impaired by *Cables1*^{TAS}, respectively.

The Cables family has two members in mammals, designated as Cables1 and Cables2, and the latter is a possible candidate with functional redundancy. *Cables2* was cloned by cross-hybridization with Cables1 and RT-PCR.[36] It has been reported that Cdk5 and Abl1 associate with Cables2, similar to Cables1. Furthermore, Cables2 is expressed in a variety of tissues, including the brain. Although no data have been reported regarding colocalization of Cables1 and Cables2 expression in the brain, the effect of Cables1 dysfunction may be masked by a redundant function of Cables2 in callosal development.

Integration of adhesive interactions with directional information from attractive and repulsive cues is essential for the correct progression of callosal axons. Cables1 connects Robo-associated Abl and N-cadherin-associated β-catenin. Truncated Cable1 includes the N-terminal half (298 amino acids) of the wild-type protein (568 amino acids). Cables1 lacking the N-terminal one-third of the protein shows markedly decreased association with Abl1 compared with the wild type.[33] Although the precise localization of Abl1 interaction site(s) of Cables1 is unknown, five of the six SH3 domain-binding motifs (PXXP) in Cables1 are located in the N-terminal region. The SH3 domain regulates the kinase activity by interacting with the kinase domain.[37] Cables1[TAS] also contains PXXP domains. The function of Abl1 may be affected by binding to the truncated Cables1. The Abl family of nonreceptor tyrosine kinases consists of Abl1 and its paralog Abl2. Although Abl1-deficient mice show normal brain formation, mice lacking both Abl1 and Abl2 kinases develop neurulation defects at 11 dpc, suggesting that both kinases play fundamental roles in central nervous system development and function.[38] Therefore, truncated Cables1 may target both Abl1 and Abl2. Further studies are required to determine whether both Abl kinases contribute to the corpus callosum organization in cerebral cells expressing Cables1 after 15 dpc and whether truncated Cable1 impairs the functions of both Abl kinases.

In conclusion, the results presented here clearly indicated that ACC in TAS mice is caused by a novel mutant gene *Cables1*[TAS]. Although the molecular mechanisms underlying the observed effects of truncated Cables1 and its related proteins are unclear, these findings will contribute to our understanding of corpus callosum development.

DISCLOSURE/CONFLICT OF INTEREST
The authors declare no conflict of interest.

1. Aboitiz F, Scheibel AB, Fisher RS, *et al*. Fiber composition of the human corpus callosum. Brain Res 1992;598:143–153.
2. Livy DJ, Schalomon PM, Roy M, *et al*. Increased axon number in the anterior commissure of mice lacking a corpus callosum. Exp Neurol 1997;146:491–501.
3. Richards LJ, Plachez C, Ren T. Mechanisms regulating the development of the corpus callosum and its agenesis in mouse and human. Clin Genet 2004;66:276–289.
4. Guillem P, Fabre B, Cans C, *et al*. Trends in elective terminations of pregnancy between 1989 and 2000 in a French county (the Isère). Prenat Diagn 2003;23:877–883.
5. Wang LW, Huang CC, Yeh TF. Major brain lesions detected on sonographic screening of apparently normal term neonates. Neuroradiology 2004;46:368–373.
6. Bodensteiner J, Schaefer GB, Breeding L, *et al*. Hypoplasia of the corpus callosum: a study of 445 consecutive MRI scans. J Child Neurol 1994;9:47–49.
7. Jeret JS, Serur D, Wisniewski K, *et al*. Frequency of agenesis of the corpus callosum in the developmentally disabled population as determined by computerized tomography. Pediatr Neurosci 1985-1986;12:101–103.
8. Barkovich AJ, Norman D. Anomalies of the corpus callosum: correlation with further anomalies of the brain. AJR Am J Roentgenol 1988;151:171–179.
9. Donahoo AL, Richards LJ. Understanding the mechanisms of callosal development through the use of transgenic mouse models. SeminPediatr Neurol 2009;16:127–142.
10. Zembrzycki A, Griesel G, Stoykova A, *et al*. Genetic interplay between the transcription factors Sp8 and Emx2 in the patterning of the forebrain. Neural Dev 2007;30:2–8.
11. Jones L, López-Bendito G, Gruss P, *et al*. Pax6 is required for the normal development of the forebrain axonal connections. Development 2002;129:5041–5052.
12. Hide T, Hatakeyama J, Kimura-Yoshida C, *et al*. Genetic modifiers of otocephalic phenotypes in Otx2 heterozygous mutant mice. Development 2002;129:4347–4357.
13. Wahlsten D, Bishop KM, Ozaki HS. Recombinant inbreeding in mice reveals thresholds in embryonic corpus callosum development. Genes Brain Behav 2006;5:170–188.
14. Kadowaki M, Nakamura S, Machon O, *et al*. N-cadherin mediates cortical organization in the mouse brain. Dev Biol 2007;304:22–33.
15. Shu T, Sundaresan V, McCarthy MM, *et al*. Slit2 guides both precrossing and postcrossingcallosal axons at the midline in vivo. J Neurosci 2003;23:8176–8184.
16. Andrews W, Liapi A, Plachez C, *et al*. Robo1 regulates the development of major axon tracts and interneuron migration in the forebrain. Development 2006;133:2243–2252.
17. Serafini T, Colamarino SA, Leonardo ED, *et al*. Netrin-1 is required for commissural axon guidance in the developing vertebrate nervous system. Cell 1996;87:1001–1014.
18. Fazeli A, Dickinson SL, Hermiston ML, *et al*. Phenotype of mice lacking functional Deleted in colorectal cancer (Dcc) gene. Nature 1997;386:796–804.
19. Ren T, Zhang J, Plachez C, *et al*. Diffusion tensor magnetic resonance imaging and tract-tracing analysis of Probst bundle structure in Netrin1- and DCC-deficient mice. J Neurosci 2007;27:10345–10349.
20. Raper JA. Semaphorins and their receptors in vertebrates and invertebrates. Curr Opin Neurobiol 2000;10:88–94.
21. Piper M, Plachez C, Zalucki O, *et al*. Neuropilin 1-Sema signaling regulates crossing of cingulate pioneering axons during development of the corpus callosum. Cereb Cortex 2009;19(Suppl 1):i11–i21.
22. Mendes SW, Henkemeyer M, Liebl DJ. Multiple Eph receptors and B-class ephrins regulate midline crossing of corpus callosum fibers in the developing mouse forebrain. J Neurosci 2006;26:882–892.
23. Woychik RP, Alagramam K. Insertional mutagenesis in transgenic mice generated by the pronuclear microinjection procedure. Int J Dev Biol 1998;42:1009–1017.
24. Jaenisch R. Transgenic animals. Science 1998;240:1468–1474.
25. Mizuno S, Mizobuchi A, Iseki H, *et al*. A novel locus on proximal chromosome 18 associated with agenesis of the corpus callosum in mice. Mamm Genome 2010;21:525–533.

26. Iijima S, Tanimoto Y, Mizuno S, *et al*. Effect of different culture conditions on establishment of embryonic stem cells from BALB/cAJ and NZB/BINJ mice. Cell Reprogram 2010;12:679–688.

27. Zukerberg LR, DeBernardo RL, Kirley SD, *et al*. Loss of cables, a cyclin-dependent kinase regulatory protein, is associated with the development of endometrial hyperplasia and endometrial cancer. Cancer Res 2004;64:202–208.

28. Kirley SD, D'Apuzzo M, Lauwers GY, *et al*. The Cables gene on chromosome 18Q regulates colon cancer progression in vivo. Cancer Biol Ther 2005;4:861–863.

29. Lee HJ, Sakamoto H, Luo H, *et al*. Loss of CABLES1, a cyclin-dependent kinase-interacting protein that inhibits cell cycle progression, results in germline expansion at the expense of oocyte quality in adult female mice. Cell Cycle 2007;6:2678–2684.

30. Matsuoka M, Matsuura Y, Semba K, *et al*. Molecular cloning of a cyclin-like protein associated with cyclin-dependent kinase 3 (cdk 3) in vivo. Biochem Biophys Res Commun 2000;273:442–447.

31. Tsuji K, Mizumoto K, Yamochi T, *et al*. Differential effect of ik3-1/cables on p53- and p73-induced cell death. J Biol Chem 2002;277:2951–2957.

32. Park do Y, Sakamoto H, Kirley SD, *et al*. The Cables gene on chromosome 18q is silenced by promoter hypermethylation and allelic loss in human colorectal cancer. Am J Pathol 2007;171:1509–1519.

33. Zukerberg LR, Patrick GN, Nikolic M, *et al*. Cables links Cdk5 and c-Abl and facilitates Cdk5 tyrosine phosphorylation, kinase upregulation, and neurite outgrowth. Neuron 2000;26:633–646.

34. Rhee J, Buchan T, Zukerberg L, *et al*. Cables links Robo-bound Abl kinase to N-cadherin-bound beta-catenin to mediate Slit-induced modulation of adhesion and transcription. Nat Cell Biol 2007;9:883–892.

35. Shu T, Richards LJ. Cortical axon guidance by the glial wedge during the development of the corpus callosum. J Neurosci 2001;21:2749–2758.

36. Sato H, Nishimoto I, Matsuoka M. ik3-2, a relative to ik3-1/cables, is associated with cdk3, cdk5, and c-abl. Biochim Biophys Acta 2002;1574:157–163.

37. Mayer BJ, Baltimore D. Mutagenic analysis of the roles of SH2 and SH3 domains in regulation of the Abl tyrosine kinase. Mol Cell Biol 1994;14:2883–2894.

38. Koleske AJ, Gifford AM, Scott ML, *et al*. Essential roles for the Abl and Arg tyrosine kinases in neurulation. Neuron 1998;21:1259–1272.

Simple generation of albino C57BL/6J mice with G291T mutation in the tyrosinase gene by the CRISPR/Cas9 system

Seiya Mizuno · Tra Thi Huong Dinh · Kanako Kato · Saori Mizuno-Iijima ·
Yoko Tanimoto · Yoko Daitoku · Yoshikazu Hoshino · Masahito Ikawa ·
Satoru Takahashi · Fumihiro Sugiyama · Ken-ichi Yagami

Abstract Single nucleotide mutations (SNMs) are associated with a variety of human diseases. The CRISPR/Cas9 genome-editing system is expected to be useful as a genetic modification method for production of SNM-induced mice. To investigate whether SNM-induced mice can be generated by zygote microinjection of CRISPR/Cas9 vector and single-stranded DNA (ssDNA) donor, we attempted to produce albino C57BL/6J mice carrying the *Tyr* gene SNM (G291T) from pigmented C57BL/6J zygotes. We first designed and constructed a CRISPR/Cas9 expression vector for the *Tyr* gene (*px330-Tyr-M*). DNA cleavage activity of *px330-Tyr-M* at the target site of the *Tyr* gene was confirmed by the EGxxFP system. We also designed an ssDNA donor for homology-directed repair (HDR)-mediated gene modification. The *px330-Tyr-M* vector and ssDNA donor were co-microinjected into the pronuclei of 224 one-cell-stage embryos derived from C57BL/6J mice. We obtained 60 neonates, 28 of which showed the ocular albinism and absence of coat pigmentation. Genomic sequencing analysis of the albino mice revealed that the target of SNM, G291T in the *Tyr* gene, occurred in 11 mice and one founder was homozygously mutated. The

remaining albino founders without *Tyr* G291T mutation also possessed biallelic deletion and insertion mutants adjacent to the target site in the *Tyr* locus. Simple production of albino C57BL/6J mice was provided by C57BL/6J zygote microinjection with *px330-Tyr-M* DNA vector and mutant ssDNA (*G291T* in *Tyr*) donor. A combination of CRISPR/Cas9 vector and optional mutant ssDNA could be expected to efficiently produce novel SNM-induced mouse models for investigating human diseases.

S. Mizuno · T. T. H. Dinh · K. Kato · S. Mizuno-Iijima ·
Y. Tanimoto · Y. Daitoku · Y. Hoshino · S. Takahashi ·
F. Sugiyama (✉) · K. Yagami
Laboratory Animal Resource Center, University of Tsukuba,
1-1-1 Tennodai, Tsukuba 305-8575, Japan
e-mail: bunbun@md.tsukuba.ac.jp

M. Ikawa
Research Institute for Microbial Diseases, Osaka University,
Suita, Osaka, Japan

Introduction

Gene knockout (KO) mice produced by gene targeting methods are essential tools for investigating endogenous gene function. In such targeting methods, genetic mutations are introduced by spontaneous homologous recombination in mouse embryonic stem cells (mESc) (Doetschman et al. 1987). Gene KO mice are generated by the production of germline chimeras derived from specific gene-mutated mESc (Capecchi 2005). Although reliable, this method is laborious, costly, and time consuming. In contrast, genome editing with engineered DNA nucleases induces site-directed gene mutations by the direct injection of DNA or RNA of site-specific engineered nucleases into fertilized oocytes. It has been reported that 3 kinds of engineered nucleases (ZFN, TALENs, and CRISPR/Cas) are useful for producing knockout (KO) mice (Carbery et al. 2010; Sung et al. 2013; Wang et al. 2013). Therefore, these new technologies are expected to be useful for producing gene-modified animals.

The bacterial type II Clustered Regularly Interspaced Short Palindromic Repeat (CRISPR) and CRISPR-associated protein 9 (Cas9) system, which consists of the Cas9

DNA nuclease, CRISPR RNA (crRNA), and trans-activating crRNA (tracrRNA), have been developed as a genome-editing method (Wiedenheft et al. 2012). A combination of crRNA-tracrRNA fusion transcripts referred to as guide RNA (gRNA) and Cas9 further facilitates genome editing (Mali et al. 2013). The gRNA contains a region of approximately 20 nucleotides (nt) homologous to the target DNA and the region recruiting Cas9 that elicits site-specific double-strand DNA breaks (DSB). In mouse zygotes, the CRISPR/Cas9 system generates KO alleles through site-specific DSB repair, which causes different and unpredictable insertions or deletions of various sizes by non-homologous end joining (NHEJ). Furthermore, optional substitution and insertion mutations in the targeted allele are generated by homology-directed repair (HDR) using the CRISPR/Cas9 system combined with a single-stranded DNA (ssDNA) donor (Wang et al. 2013; Yang et al. 2013).

Single nucleotide polymorphisms and mutations (SNPs and SNMs, respectively) are associated with a variety of human diseases (Imamura et al. 2012; Kou et al. 2011; Rademakers et al. 2007). However, as the generation of SNMs is more technically difficult than standard null mutations, the use of SNM-induced mice has been limited. To our knowledge, there have been no previous reports of the generation of SNM-induced mice with an apparently abnormal phenotype by the CRISPR/Cas9 system. A missense substitution, G291T (Arg77Leu), at the alternative 5′ splice donor site for exon 1 of the Tyrosinase (Tyr) gene was shown to cause oculocutaneous albinism in pigmented C57BL/6J mice (Le et al. 1996). Therefore, this missense mutation is convenient for evaluating the effectiveness of the CRISPR/Cas9 system on the production of SNM-induced mice.

In the present study, we first constructed CRISPR/Cas9 including the target DNA site of the Tyr gene and a mutant ssDNA donor for G291T point mutation. Second, the nuclease activity of the CRISPR/Cas9 construct at the target DNA site of the Tyr gene was examined by the EGxxFP system in HEK293T cells. Third, the CRISPR/Cas9 construct and mutant ssDNA donor were injected simultaneously into the pronuclei of C57BL/6J eggs. Fourth, the coat color phenotypes and first exon sequences of the Tyr gene were investigated in offspring derived from microinjected zygotes. Finally, we confirmed that Tyr G291T mutation in gene-modified mouse was precisely transmitted to the next generation.

Materials and methods

Animals

C57BL/6J and ICR mice were purchased from Charles River Laboratories Japan (Kanagawa, Japan) and CLEA Japan (Tokyo, Japan), respectively. Animals were maintained as described previously (Mizuno et al. 2010), and animal experiments were carried out humanely in accordance with the Regulations for Animal Experiments of the University of Tsukuba and Fundamental Guidelines for Proper Conduct of Animal Experiment and Related Activities in Academic Research Institutions under the jurisdiction of the Ministry of Education, Culture, Sports, Science, and Technology of Japan and with approval from the Institutional Animal Experiment Committee of our university.

Vector construction

The px330 vector (Addgene plasmid 42230) was a gift from Dr. Feng Zhang (Cong et al. 2013). Tyr-M CRISPR F (5′-ca ccGGGTGGATGACCGTGAGTCC-3′) and Tyr-M CRISPR R (5′-aaacGGACTCACGGTCATCCACCC-3′) oligo DNAs were annealed by the standard method, and annealed DNA was purified by ethanol precipitation. This short double-stranded DNA was inserted into the BbsI restriction site in the px330 vector by Ligation high Ver.2 (Toyobo, Osaka, Japan). This plasmid was designated as px330-Tyr-M.

The single-stranded oligo DNA was obtained from Life Technologies (Carlsbad, CA).

For the EGxxFP system, part of exon 1 of the Tyr gene was amplified with PrimeSTAR® GXL DNA Polymerase (Takara Bio, Shiga, Japan) and the following primers:

Tyr-EGxxFP-F: 5′-CAACCACTGAGGATCGCTTCAT GGGCAAAATCAAT-3′,
Tyr-EGxxFP-R: 5′-GGTCAGCTTGCCGATTTGTTGG CAAAAGA ATGCTG-3′.

The PCR product was purified with a Fast Gene Gel/PCR Extraction Kit (Nippon Genetics Co., Ltd., Tokyo, Japan) and inserted into pCX-EGxxFP using an In-Fusion HD Cloning Kit (Takara Bio). This plasmid was designated as pCX-EGxxFP-Tyr-M. These two vectors, px330-Tyr-M and pCX-EGxxFP-Tyr-M, were purified with a Fast Gene Plasmid Mini Kit (Nippon Genetics).

Transfection

The px330-Tyr-M and pCX-EGxxFP-Tyr-M vectors were transfected into HEK293T cells by LipofectAMINE LTX (Life Technologies). EGFP fluorescence in HEK293T cells was observed by fluorescence microscopy (DMLB; Leica Microsystems GmbH, Wetzlar, Germany) with appropriate filter sets (excitation: 480 ± 40 nm and emission: 527 ± 30 nm band pass filters).

Microinjection

Female C57BL/6J mice were injected with pregnant mare serum gonadotropin (PMSG) and human chorionic

gonadotropin (hCG) with a 48-h interval, and mated with male C57BL/6J mice. The fertilized one-cell embryos were collected from the oviducts. Then, 5 ng/μl of *px330-Tyr-M DNA* vector (circular) and 10 ng/μl ssDNA donor were injected into the pronuclei of these one-cell-stage embryos according to standard protocols (Gordon and Ruddle 1981). The injected one-cell embryos were then transferred into pseudopregnant ICR mice.

Genomic PCR and sequence analysis

The screening of founder mice and examination of off-target effect were performed by PCR and direct sequencing using DNA obtained from the tail. PCR was performed with PrimeSTAR® GXL DNA Polymerase (Takara Bio) and the following primers:

Cas9 detection primer F: 5′-AGTTCATCAAGCCCATCCTG-3′
Cas9 detection primer R: 5′-GAAGTTTCTGTTGGCGAAGC-3′
Tyr genotyping F: 5′-GCTTCATGGGCAAAATCAAT-3′
Tyr genotyping R: 5′-TTGTTGGCAAAAGAATGCTG-3′
Off-target detection primer 1 F: 5′-GAAGGCAGGTGGATCTAACG-3′
Off-target detection primer 1 R: 5′-GGGCCACTGCTATCAGCTAC-3′
Off-target detection primer 2 F: 5′-CTCAGCCATCCCAAGGTAAA-3′
Off-target detection primer 2 R: 5′-CAGCCCACAGGACCATTACT-3′
Off-target detection primer 3 F: 5′-GGTTGGGGGAAGATGGTTAT-3′
Off-target detection primer 3 R: 5′-GACAATTGAAGGTGGGCATT-3′
Off-target detection primer 4 F: 5′-TGCTAGACCGAAAAGCAGGT-3′
Off-target detection primer 4 R: 5′-CCCTTTCTTGTGCTCTCTGG-3′
Off-target detection primer 5 F: 5′-TAGGGGCAATTCCCATACAG-3′
Off-target detection primer 5 R: 5′-CAGCAGGTTTGACCACAATG-3′

The PCR products were purified with a Fast Gene Gel/PCR Extraction Kit, and sequences were analyzed using an Applied Biosystems 3130 Genetic Analyzer (Life Technologies) with a BigDye® Terminator v3.1 Cycle Sequencing Kit (Life Technologies) and the primers as described above.

Mutant genome sequences detected by direct sequencing were analyzed by cloned sequencing. Purified PCR products were subcloned into the *pCR4* vector and sequenced using the M13-RV primer.

Results

Construction of Tyr-CRISPR/Cas9 expression vector

Le et al. (1996) reported that spontaneous mutant C57BL/6J-*Try*[c-2J] mice showed an albino phenotype because of a guanine (G) to thymine (T) point mutation at position 291 in the *Tyr* gene. The nucleotide T at position 291 cannot function as an alternative 5′ splice donor site for exon 1 and generates nonfunctional tyrosinase protein for melanin synthesis.

To introduce this point mutation with the CRISPR/Cas9 system, we first determined an appropriate CRISPR target site. As the CRISPR/Cas9 system recognizes and cleaves genomic sites of the form G-N(20)-GG, we selected positions 279–301 of the *Tyr* gene (Fig. 1). In addition, we also designed a 91-nt ssDNA donor (Chen et al. 2011) for HDR-mediated genome mutation; the nucleotide T was placed between 45-nt 5′- and 45-nt 3′-homology arms derived from positions 246–290 and 292–336 of the *Tyr* gene, respectively (Fig. 1). The *px330* vector was used to express gRNA for the targeted region of *Tyr* and Cas9 protein in mouse zygotes (Cong et al. 2013). This vector contains two elements, gRNA under the control of the by U6 promoter and *Cas9* cDNA under the control of the by CBh promoter. The 20-bp double-stranded DNA (dsDNA) derived from positions 279–298 of the *Tyr* gene was inserted into *px330*, and the resultant plasmid was designated as *px330-Tyr-M*.

Activity of the *px330-Tyr-M* vector

The cleavage activity of the *px330-Tyr-M* vector was confirmed by the EGxxFP system (Mashiko et al. 2013). The *pCX-EGxxFP* vector includes a multi-cloning site (MCS) between two cDNA fragments containing stop sequences, *N-* and *C-EGFP*, which were derived from positions 1–600 and 120–720 of full-length *EGFP*, respectively, which possessed 480-bp homology sequences. Exon 1 of the *Tyr* gene was inserted into MCS in *pCX-EgxxFP*, and the resultant vector was designated as *pCX-EGxxFP-Tyr-M*. Accordingly, functional EGFP is not expressed from intact *pCX-EGxxFP-Tyr-M*. When the *Tyr* fragment in *pCX-EGxxFP-Tyr-M* is cleaved by the *px330-Tyr-M* vector, full-length functional EGFP is produced by HDR (Fig. 2a) and is expressed by the *CX* promoter activity. To confirm the above mechanism, both *pCX-EGxxFP-Tyr-M* and *px330-Tyr-M* vectors were co-transfected into HEK293T cells, and strong EGFP signals were observed in co-transfected cells (Fig. 2b). In contrast, very weak and no EGFP signals were detected in *pCX-EGxxFP-Tyr-M*-transfected cells (Fig. 2c) and non-transfected cells (Fig. 2d), respectively. These results indicated that the
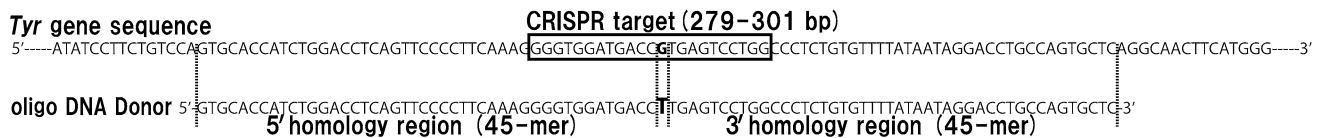
Tyr gene sequence

CRISPR target (279–301 bp)

5′-----ATATCCTTCTGTCCAGTGCACCATCTGGACCTCAGTTCCCCTTCAAAG|GGGTGGATGACCG**G**TGAGTCCTGG|CCCTCTGTGTTTTATAATAGGACCTGCCAGTGCTCAGGCAACTTCATGGG-----3′

oligo DNA Donor 5′-GTGCACCATCTGGACCTCAGTTCCCCTTCAAAGGGGTGGATGACC**T**TGAGTCCTGGCCCTCTGTGTTTTATAATAGGACCTGCCAGTGCTC-3′

5′ homology region (45-mer)   3′ homology region (45-mer)

Fig. 1 CRISPR target site in the *Tyr* gene. In the *upper sequence*, the CRISPR target sequence is position 279–301 bp of the *Tyr* gene (*boxed*). The 91-nt oligo DNA sequences are shown in the *lower sequence*. The *boldface* **G** in the *upper sequence* and **T** in the *lower sequence* indicate the target single nucleotide mutation
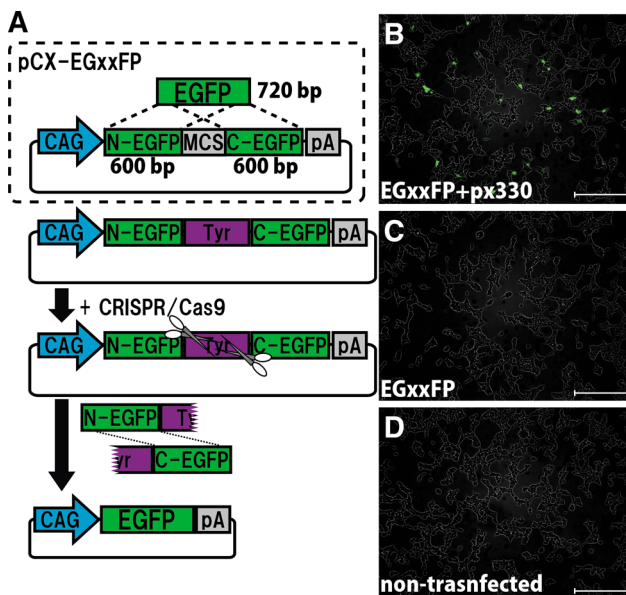

Fig. 2 EGxxFP system for checking CRISPR activity. **a** The multi-cloning site (MCS, *gray box*) containing a stop codon is located between the 600-bp N-terminal *EGFP* (*N-EGFP*) and 600-bp C-terminal *EGFP* (*C-EGFP*) fragments in the *pCX-EGxxFP* plasmid (*broken line box*). Exon 1 of the *Tyr* gene (*purple box*) was inserted into the MCS in *pCX-EGxxFP*. After double-strand break by CRISPR (scissors) and homologous recombination between shared 500-bp in *N*- and *C-EGFP* fragments (*broken line*), functional EGFP was reconstructed. **b** The robust EGFP signals were seen in both *pCX-EGxxFP-Tyr-M* and *px330-Tyr-M* co-transfected HEK293T cells. Very weak EGFP signals (**c**) and no signal (**d**) were observed in only *pCX-EGxxFP-Tyr-M*-transfected and non-transfected HEK293T cells. *Scale bars* 300 μm

px330-Tyr-M vector has the ability to cleave the *Tyr* genome fragment.

Co-microinjection of *Tyr*-CRISPR and mutant ssDNA donor into mouse zygotes

To induce the SNM (*G291T*) in the *Tyr* gene, 5 ng/μl of the *px330-Tyr-M DNA* vector (circular) and 10 ng/μl of the mutant ssDNA donor were co-microinjected into the pronuclei of 224 one-cell-stage embryos obtained from C57BL/6J mice. No morphological abnormalities were observed in 205 of 224 one-cell embryos immediately after microinjection (~90 %). These one-cell embryos with normal appearance were transferred into the oviducts of

Table 1 Production of C57BL6/J albino mice

Injected DNA	Injected zygotes	Transferred embryos	No. of postnatal mice	
			Coat color	
px330-Tyr-M (5 ng/μl)	224	205	Black	18 (30.0 %)[a]
			Mosaic	14 (23.3 %)[b]
ssDNA donor (10 ng/μl)			Albino	28 (46.7 %)[c]
			Total	60

[a] No. of black mice/no. of postnatal mice

[b] No. of mosaic mice/no. of postnatal mice

[c] No. of albino mice/no. of postnatal mice

pseudopregnant recipient ICR mice, and 60 neonates, including 28 with depigmented eyes, were obtained (Table 1). The 28 mice with depigmented eyes survived and had a white coat over the whole body (Fig. 3a; Supplementary Fig. 1) and pink fully translucent irises (Fig. 3b). Unexpectedly, fourteen mice with a black and white mosaic coat pattern (Fig. 3a; Supplementary Fig. 1) were also obtained (Table 1). These results suggested that microinjection with *px330-Tyr-M* vector and the mutant ssDNA donor can induce complete and/or mosaic albino phenotypes in C57BL/6J mice. The appearance of mosaicism appeared to have been due to mutation events, occurring after the first or later divisions of the embryos.

Genomic sequences of founder albino mouse lines

To determine whether the *px330-Tyr-M DNA* vector was integrated into the chromosomes, we performed PCR assay with founder mouse genomic DNA and a primer pair for Cas9 detection. Cas9 PCR products were detected in only one founder mice (Table 2). Genomic sequence of this albino mouse was not analyzed, because it was assumed that the modification of its genome was continued by transgenic gRNA and *Cas9* expression. Sequencing analyses with 27 albino mice showed that optional substitution (*G291T*) was induced in 11 mice (Table 2). Surprisingly, albino founder #19 carried the optional substitution in both alleles (Fig. 4a). Ten of 11 albino founders carrying the *Tyr* G291T mutation (#6, #8, #10, #14, #18–20, #22, #25, and #26) also possessed monoallelic deletion mutations adjacent to the target site in the *Tyr* locus (Fig. 4b). The

Fig. 3 C57BL/6J mice with albino phenotype. One week after birth, mice with completely white (two of 28)/black coats and three mosaic mice with black and white coats (two of the mosaic founders) were obtained (**a**). Pink irises (*white box*) and white coat color in an 8-week-old albino C57BL/6J mouse (albino founder #1) are shown (**b**)
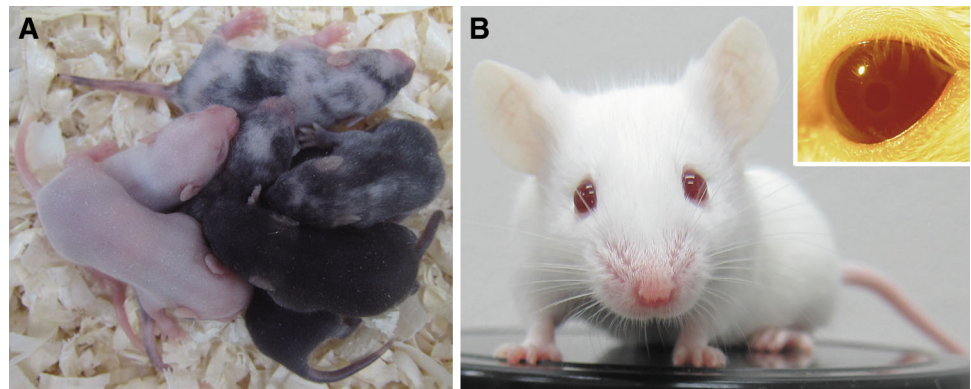
Table 2 Mutation alleles in albino mice

No. of postnatal mice		Detected mutation alleles	
Albino	Without px330 integration		
28	27 (96.4 %)[a]	NHEJ	16 (59.3 %)[b]
		NHEJ/SNM (*G291T*)	10 (37.0 %)[c]
		SNM (*G291T*)	1 (3.7 %)[d]
		Total	27

[a] No. of albino mice without px330 integration/no. of albino mice

[b] No. of mice with NHEJ alleles/no. of albino mice without px330 integration

[c] No. of mice with both NHEJ and SNM alleles/no. of albino mice without px330 integration

[d] No. of mice with SNM alleles/no. of albino mice without px330 integration

remaining 16 albino founders had biallelic deletion/insertion mutations in the *Tyr* locus (Table 2; Supplementary Fig. 2). Unexpectedly, albino founders #14, #24, and #25 were mosaic with more than three alleles (Fig. 4b; Supplementary Fig. 2). Although identical indel mutations were detected in several alleles (e.g., deletion G295 in 4 alleles and deletion GAGT293-296 in 5 alleles), the optional substitution occurred most frequently (12 alleles). Hence, *G291T* in the *Tyr* gene was considered to be induced by HDR-mediated gene mutation using with *px330-Tyr-M DNA* vector and ssDNA donor. Moreover, these results indicated that HDR-mediated gene mutation occurred concurrently with NHEJ-mediated gene mutation in mouse zygotes.

Examination of off-target effects in an albino founder

We then surveyed the off-target effects in 4 albino founders, #19 carried the optional substitution in both alleles, and # 6, #8, and #10 carried the optional substitution and deletion mutant alleles. By the pronuclear injection of circular CRISPR plasmid DNA, off-target effects were observed at several genome sites that exactly matched 16

bases at the 3′ end including the PAM (NGG) sequence (N can be A, G, C, or T) (Mashiko et al. 2014). Therefore, we selected off-target candidate #1 that exactly matched to the CRISPR target sequence at 16 bases at the 3′ end. Furthermore, we selected 4 off-target candidates (#2 to #5) who showed high homology to the CRISPR target site (16-to 20-base match) (Supplemental Fig. 3). The genome sequence of these 5 off-target candidates were confirmed by direct sequencing analysis. As the result, no mutation was found in any of the off-targets. The result suggested that the optional substitution might be induced with little or no off-target effects.

Inheritance of induced SNM

To confirm whether the SNM induced by *px330-Tyr-M DNA* vector and ssDNA donor could be inherited, albino founder male #1 was crossed with a wild-type C57BL/6J female. We obtained 8 F$_1$ mice with black coat color. Genotyping sequence analyses revealed that 5 and 3 mice carried heterozygous *Tyr* G292T, and heterozygous *Tyr* deletion GTGAG291-295, respectively (Fig. 5). Then, seven F$_2$ mice were obtained from intercross of heterozygous SNM mice. As the result, we obtained 2 albino mice and 5 black mice (Fig. 5). As expected, homozygous *Tyr* G291T mutations were detected in both of 2 F$_2$ albino mice (data not shown). These results indicated that the optional substitution could be precisely transmitted to the next generation. Moreover, we reconfirmed that this SNM resulted in the albino phenotype in mice.

Discussion

The results of the present study demonstrated induction of albino phenotypes by pronuclear microinjection of zygotes with circular DNA expressing *Cas9* and gRNA along with mutant ssDNA donor. Interestingly, eleven albino founders

Fig. 4 Mutant genomic sequences in albino mice with targeted SNMs. **a** Genomic sequence of CRISPR target site in C57BL/6J wild-type and albino #19 mice. *Black box* indicates the targeted SNM. **b** The *red letters* indicate the CRISPR target site. The *large letter* "G" in *red* is the target single nucleotide. The *green letters* indicate mutant genomic sequences in albino mice. The targeted SNM (*large letter* "T" in *green*) was found in 11 albino mice. The other allele had deletion mutations

A

```
      G G G T G G A T G A C C G T G A G T C C T G G
Wild Type

      G G G T G G A T G A C C T T G A G T C C T G G
Albino #19
```

B

```
Wild Type   CCCTTCAAAGGGGTGGATGACCGTGAGTCCTGGCCCTCTGTGTTTTA

Albino #1   CCCTTCAAAGGGGTGGATGACCTTGAGTCCTGGCCCTCTGTGTTTTA
            CCCTTCAAAGGGGTGGATGACC-----TCCTGGCCCTCTGTGTTTTA

Albino #6   CCCTTCAAAGGGGTGGATGACCTTGAGTCCTGGCCCTCTGTGTTTTA
            CCCTTCAAAGGGGTGGATGACC------------CTCTGTGTTTTA

Albino #8   CCCTTCAAAGGGGTGGATGACCTTGAGTCCTGGCCCTCTGTGTTTTA
            CCCTTCAAAGGGGTGGATGACCGTG-GTCCTGGCCCTCTGTGTTTTA

Albino #10  CCCTTCAAAGGGGTGGATGACCTTGAGTCCTGGCCCTCTGTGTTTTA
            CCCTTCAAAGGGGTGGATGACCGT--------------GTGTTTTA

            CCCTTCAAAGGGGTGGATGACCTTGAGTCCTGGCCCTCTGTGTTTTA
Albino #14  CCCTTCAAAGGGGTGGATGACCGTGAG--CTGGCCCTCTGTGTTTTA
            CCCTTC-------------------------------TGTGTTTTA

Albino #18  CCCTTCAAAGGGGTGGATGACCTTGAGTCCTGGCCCTCTGTGTTTTA
            CCCTTCAAAGGGGTGGATGACCGT---- CCTGGCCCTCTGTGTTTTA

Albino #19  CCCTTCAAAGGGGTGGATGACCTTGAGTCCTGGCCCTCTGTGTTTTA

Albino #20  CCCTTCAAAGGGGTGGATGACCTTGAGTCCTGGCCCTCTGTGTTTTA
            CCCTTCAAAGGGGTGGATGACCGTGA-TCCTGGCCCTCTGTGTTTTA

Albino #22  CCCTTCAAAGGGGTGGATGACCTTGAGTCCTGGCCCTCTGTGTTTTA
            CCCTTCAAAGGGGTGGATGACCGTGAG------CCCTCTGTGTTTTA

            CCCTTCAAAGGGGTGGATGACCTTGAGTCCTGGCCCTCTGTGTTTTA
Albino #25  CCCTTCAAAGGGGTGGATGACCTTGA-TCCTGGCCCTCTGTGTTTTA
            CCCTTCAAAGGGGTGGATGACC--------TGGCCCTCTGTGTTTTA

Albino #26  CCCTTCAAAGGGGTGGATGACCTTGAGTCCTGGCCCTCTGTGTTTTA
            CCCTTCAAAGGGGTGGATGACC--------TGGCCCTCTGTGTTTTA
```
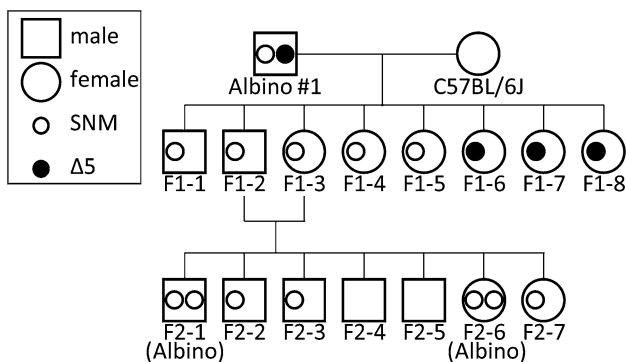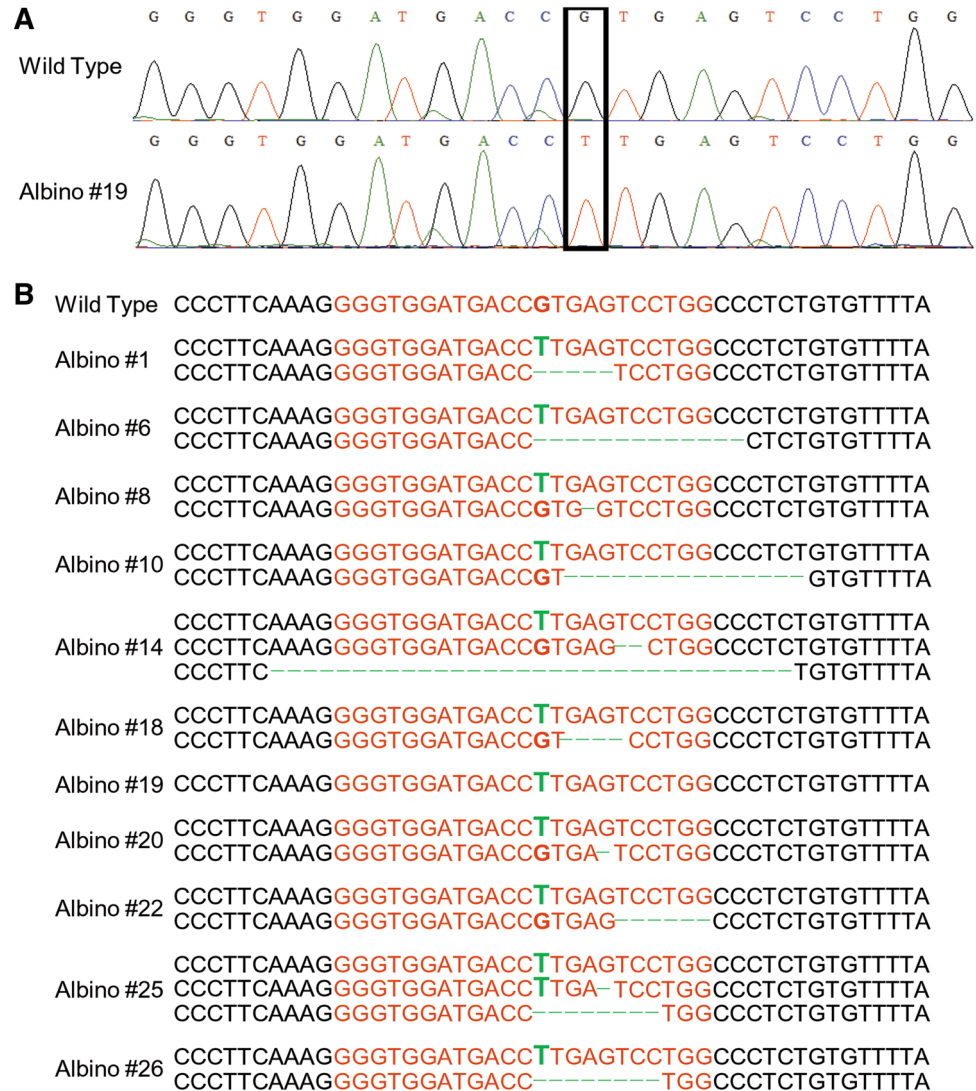
Fig. 5 Pedigree of albino founder #1 line. The *squares* and *circles* represent male and female mice, respectively. The *white* and *black small circles* mean targeted SNM and 5-bp deletion alleles, respectively. Albino phenotypes were seen in albino #1, #F$_2$-1, and #F$_2$-6

had HDR-mediated optional substitution in *Tyr* derived from wild-type C57BL/6J, and one albino founder was homozygously mutated.

Linkage studies in humans have demonstrated the involvement of SNPs and SNMs with amino acid substitutions in many diseases (Haga et al. 2002; Hirakawa et al. 2002). SNMs in mice have been developed by *N*-ethyl-*N*-nitrosourea (ENU) mutagenesis and gene targeting methods. Although numerous SNM alleles in mice have been generated by ENU mutagenesis, it is extremely difficult to find an optimal target SNM for a gene of interest (Gondo 2008). Furthermore, in gene targeting methods, it is necessary to use the Cre-loxP or FLP-FRT system to generate SNM alleles, and successful production of SNM-induced mice is highly dependent on germline competency of ES cells. In contrast, we clearly demonstrated that microinjection of zygotes with the *CRISPR/Cas9* vector and mutant ssDNA donor can readily induce target SNMs (Fig. 4). This method will, therefore, be very useful for producing mouse models of SNM-induced diseases.

Wang et al. (2013) first reported that mice carrying gene mutation could be generated by zygote microinjection of gRNA and *Cas9* mRNA. Here, we showed that target gene mutation could be induced by circular DNA (*px330* vector) microinjection. Although DNA microinjection methods raise the possibility of integration of injected DNA vectors into the chromosomes (Gordon and Ruddle 1981), Cas9 fragments in the *px330-Tyr-M DNA* vector were detected in only one founder (1/28). Circular DNA is considered to be difficult to integrate into chromosomes of mouse zygotes compared with linearized DNA vectors. As the preparation of DNA is easier and faster than RNA for zygote microinjection, our method is simple for producing genetically modified mice.

Very recently, Mashiko et al. (2013) reported that pronuclear microinjection off *px330* vector, containing *Cas9* expression cassette with a gene targeting gRNA expression cassette, into mouse eggs caused NHEJ-mediated mutations at a high frequency. When they targeted the *Cetn1* gene, 58.8 % (10/17) of the pups carried the mutation and six of them were homozygously mutated. In the present study, we targeted the *Tyr* gene by pronuclear microinjection of *px330-Tyr-M DNA* vector along with mutant ssDNA. Although black mice were not genotyped, at least 70.0 % (albino and mosaic founders) of the pups (42/60) could have *Tyr* albino mutation. Indel mutations with albino phenotype were observed in 43.3 % of the pups (26/60). Our results reconfirmed that pronuclear microinjection of circular plasmid expressing *Cas9* and gRNA provided highly efficient induction of NHEJ-mediated mutation. More significantly, we found HDR-mediated *Tyr* G291T mutation in 18.3 % of the pups (11/60), and one albino founder (1.6 % of the pups) was homozygously mutated. Wang et al. (2013) also generated mice with HDR-mediated precise mutations by coinjecting *Cas9* mRNA, gRNA, and ssDNA donor into the cytoplasm of one-cell-stage mouse embryos. They are consistent with our data that homologous recombination of ssDNA donor is frequently caused at the double-strand break site targeted with Cas9. Therefore, the method of pronuclear microinjection with DNA and ssDNA could be more convenient for the production of SNM-induced mice than that of cytoplasmic injection with RNA and ssDNA.

It has been reported that mosaic mice were generated with CRISPR/Cas9 system (Yang et al. 2013). In addition, mosaic phenotypes were observed in ZNF-induced animals (Hauschild-Quintern et al. 2013). Similarly, mosaic coat patterns were observed in the present study (Fig. 3a). The mice with mosaic coat patterns black and white were a lot more than we had expected. Therefore, it is necessary to pay close attention to the genotype of founder mice produced by the CRISPR/Cas9 system, with the exception of those with targeting of coat color-related genes.

On the application of gene modification with the CRISPR/Cas9 system to in vivo, many researchers have been worried about high off-target effects of the CRISPR/Cas9 system in culture cells (Fu et al. 2013). Mashiko et al. (2014) showed that very few off-target mutations occurred by pronuclear microinjection of *px330* plasmid DNA in mice. In agreement with this report, no off-target mutation was seen in 5 albino founders which carried the optional substitution. However, we just examined off-target effect for only five founders. It could be insufficient for an accurate estimate of off-target effects in our methods. Therefore, more detailed analyses of off-target effects are necessary for precisely understanding the quality of genetically modified mice with the CRISPR/Cas9 system.

Recently, albino mouse strains have been used for non-invasive studies with bioluminescence and fluorescence imaging analyses to investigate a variety of disease processes (Sadiko and Blackwell 2008; Sato et al. 2004; Sekiguchi et al. 2012). Although, pigmented C57BL/6J mice have the preferred genetic background for genetically modified mouse strains, the presence of melanin in the skin attenuates bioluminescence and fluorescence signals due to its high absorption coefficient. Moreover, individual differences in the amount of skin melanin result in misinterpretation of the actual bioluminescence and fluorescence signal. In the present study, we successfully generated albino C57BL/6J mice from pigmented C57BL/6J zygotes by simple methods using the CRISPR/Cas9 system. As many genetically modified C57BL/6J mouse stains are available with the potential for bioluminescence and fluorescence imaging analyses, the CRISPR/Cas9 system described in this study would be effective in the development of albinism in genetically modified C57BL/6J mice, similar to backcrossing with spontaneous albino C57BL/6J mice.

Additionally, Wu et al. (2013) indicated possibility of genetic correction in mice using with *Cas9* mRNA, gRNA, and ssDNA donor. Although there are still several problems to solve (e.g., off-target effect and optimizing gene transfer protocol), our and their results suggest that CRISPR-Cas9 system could be used for correcting human genetic disease in the future.

In conclusion, simple production of inheritable albino C57BL/6J mice was achieved by pronuclear microinjection of C57BL/6J zygotes with *px330-Tyr-M DNA* vector and mutant ssDNA (*G291T in Tyr*) donor. A combination of *CRISPR/Cas9* vector and optional mutant ssDNA could be expected to efficiently produce novel SNM-induced mouse models in which to investigate various human diseases.

References

Capecchi MR (2005) Gene targeting in mice: functional analysis of the mammalian genome for the twenty-first century. Nat Rev Genet 6:507–512

Carbery ID, Ji D, Harrington A, Brown V, Weinstein EJ et al (2010) Targeted genome modification in mice using zinc-finger nucleases. Genetics 186:451–459

Chen F, Pruett-Miller SM, Huang Y, Gjoka M, Duda K et al (2011) High-frequency genome editing using ssDNA oligonucleotides with zinc-finger nucleases. Nat Methods 8:753–755

Cong L, Ran FA, Cox D, Lin S, Barretto R et al (2013) Multiplex genome engineering using CRISPR/Cas systems. Science 339:819–823

Doetschman T, Gregg RG, Maeda N, Hooper ML, Melton DW et al (1987) Targetted correction of a mutant HPRT gene in mouse embryonic stem cells. Nature 330:576–578

Fu Y, Foden JA, Khayter C, Maeder ML, Reyon D et al (2013) High-frequency off-target mutagenesis induced by CRISPR-Cas nuclease in human cells. Nat Biotechnol 31:822–826

Gondo Y (2008) Trends in large-scale mouse mutagenesis: from genetics to functional genomics. Nat Rev Genet 9:803–810

Gordon JW, Ruddle FH (1981) Integration and stable germ line transmission of genes injected into mouse pronuclei. Science 214:1244–1246

Haga H, Yamada R, Ohnishi Y, Nakamura Y, Tanaka T (2002) Gene-based SNP discovery as part of the Japanese Millennium Genome Project: identification of 190,562 genetic variations in the human genome. Single-nucleotide polymorphism. J Hum Genet 47:605–610

Hauschild-Quintern J, Petersen B, Cost GJ, Niemann H (2013) Gene knockout and knockin by zinc-finger nucleases: current status and perspectives. Cell Mol Life Sci 70:2969–2983

Hirakawa M, Tanaka T, Hashimoto Y, Kuroda M, Takagi T et al (2002) JSNP: a database of common gene variations in the Japanese population. Nucleic Acids Res 30:158–162

Imamura M, Maeda S, Yamauchi T, Hara K, Yasuda K et al (2012) A single-nucleotide polymorphism in ANK1 is associated with susceptibility to type 2 diabetes in Japanese populations. Hum Mol Genet 21:3042–3049

Kou I, Takahashi A, Urano T, Fukui N, Ito H et al (2011) Common variants in a novel gene, FONG on chromosome 2q33.1 confer risk of osteoporosis in Japanese. PLoS ONE 6:e19641

Le FN, Kelsall SR, Mintz B (1996) Base substitution at different alternative splice donor sites of the tyrosinase gene in murine albinism. Genomics 37:245–248

Mali P, Yang L, Esvelt KM, Aach J, Guell M et al (2013) RNA-guided human genome engineering via Cas9. Science 339:823–826

Mashiko D, Fujihara Y, Satouh Y, Miyata H, Isotani A et al (2013) Generation of mutant mice by pronuclear injection of circular plasmid expressing Cas9 and single guided RNA. Sci Rep. 3:3355

Mashiko D, Young SA, Muto M, Kato H, Nozawa K (2014) Feasibility for a large scale mouse mutagenesis by injecting CRISPR/Cas plasmid into zygotes. Dev Growth Differ 56:122–129

Mizuno S, Mizobuchi A, Iseki H, Iijima S, Matsuda Y et al (2010) A novel locus on proximal chromosome 18 associated with agenesis of the corpus callosum in mice. Mamm Genome 21:525–533

Rademakers R, Baker M, Gass J, Adamson J, Huey ED et al (2007) Phenotypic variability associated with progranulin haploinsufficiency in patients with the common 1477C→T (Arg493X) mutation: an international initiative. Lancet Neurol 6:857–868

Sadiko RT, Blackwell TS (2008) Bioluminescence imaging modality for in vitro and in vivo gene expression. Methods Mol Biol 477:383–394

Sato A, Kaaunber B, Tolwani T (2004) In vivo bioluminescence imaging. Comp Med 54:631–634

Sekiguchi Y, Owada J, Oishi H, Katsumata T, Ikeda K et al (2012) Noninvasive monitoring of β-cell mass and fetal β-cell genesis in mice using bioluminescence imaging. Exp Anim 61:445–451

Sung YH, Baek IJ, Kim DH, Jeon J, Lee J et al (2013) Knockout mice created by TALEN-mediated gene targeting. Nat Biotechnol 31:23–24

Wang H, Yang H, Shivalila CS, Dawlaty MM, Cheng AW et al (2013) One-step generation of mice carrying mutations in multiple genes by CRISPR/Cas-mediated genome engineering. Cell 153:910–918

Wiedenheft B, Sternberg SH, Doudna JA (2012) RNA-guided genetic silencing systems in bacteria and archaea. Nature 482:331–338

Wu Y, Liang D, Wang Y, Bai M, Tang W (2013) Correction of a genetic disease in mouse via use of CRISPR-Cas9. Cell Stem Cell 13:659–662

Yang H, Wang H, Shivalila CS, Cheng AW, Shi L et al (2013) One-step generation of mice carrying reporter and conditional alleles by CRISPR/Cas-mediated genome engineering. Cell 154:1370–1379